

Thermodynamic Development of Corrosion Rate Modeling in Iron Phosphate Glasses

Fuel Cycle R&D

Mark Schlesinger,
Missouri University of Science and
Technology (Missouri S&T)

In collaboration with:
Missouri S&T
Brigham Young University

John Vienna, Technical POC
Jim Bresee, Federal Technical POC

FINAL REPORT

THERMODYNAMIC DEVELOPMENT OF CORROSION RATE MODELING IN IRON PHOSPHATE GLASSES

NEUP Project CFP-09-800

Mark E. Schlesinger and Richard K. Brow
Department of Materials Science and Engineering
Missouri University of Science and Technology
October 31, 2011

Participants: Mark E. Schlesinger, Missouri University of Science and Technology (Missouri S&T)

Richard K. Brow, Missouri S&T

Julia E. Medvedeva, Missouri S&T

Melodie Schmitt, Missouri S&T

Li Na Ma, Missouri S&T

Elizabeth Buchheit, Missouri S&T

Alex Wilmot, Missouri S&T

Xiao-Ming Chang, Missouri S&T

Juliana Boerio-Goates, Brigham Young University (BYU)

Brian F. Woodfield, BYU

Quan Shi, BYU

Abstract

A two-year research program investigated links between the thermodynamic properties of phosphate glasses and their corrosion rates in different solutions. Glasses in the $\text{Na}_2\text{O-CaO-P}_2\text{O}_5$ and $\text{Na}_2\text{O-Fe}_2\text{O}_3\text{-PO}_5$ systems were prepared and characterized. These glasses were then exposed in bulk and powder form to acid (0.1M HCl), basic (0.1M KOH) and neutral (deionized water) solutions at varying exposure times and temperatures. Analysis of the solution and the glass after exposure determined the rate and type of corrosion that occurred. Simultaneously, efforts were made to determine the thermodynamic properties of solid iron phosphate compounds. This included measurement of low-temperature (5–300 K) heat capacities, measured at Brigham Young University; the attempted use of a Parr calorimeter to measure ambient-temperature enthalpies of formation; and attempted measurement of high-temperature heat capacities. Only the first of the three tasks was successfully accomplished. In lieu of experimental measurement of enthalpies of formation, first-principles calculation of enthalpies of formation was performed at Missouri S&T; these results will be used in subsequent modeling efforts.

Project Objective

The superior corrosion resistance of iron phosphate-based glasses enhances their potential as a fixation medium for high-level nuclear waste, in particular fission-product oxides. Modeling the corrosion rate of these glasses as a function of controllable variables (Fe/P ratio, $\text{Fe}^{3+}/\text{Fe}^{2+}$ ratio, waste loading) requires an improved database for long-term corrosion kinetics and the thermodynamic properties of the glasses. A two-part research program will determine (i) corrosion kinetic parameters of iron phosphate glasses with different chemistries and simulated waste loading levels, and (ii) the thermodynamic properties of iron phosphate compounds, in particular the enthalpies and Gibbs energies of formation.

Objective 1 – Corrosion Kinetics of $\text{Na}_2\text{O}-\text{CaO}-\text{P}_2\text{O}_5$ and $\text{Na}_2\text{O}-\text{FeO}_x-\text{P}_2\text{O}_5$ Glasses

I. Introduction

Phosphate glasses have been developed for nuclear waste encapsulation and for biomedical applications. The dissolution behavior depends on the type of phosphate anions that constitute the glass structure and the associated metal cations. The objective of this study was to characterize the dissolution behavior of a series of $x\text{Na}_2\text{O}-x\text{CaO}-(100-2x)\text{P}_2\text{O}_5$ ($x=24\sim 31$ mol%) glasses and $\text{Na}_2\text{O}-x\text{Fe}_2\text{O}_3-(100-2x)\text{P}_2\text{O}_5$ ($\text{O}/\text{P} = 3.0\sim 3.5$) glasses in the meta- to polyphosphate range. Dissolution rates were determined from weight loss measurements and ion concentrations in solutions. The effects of experimental conditions on dissolution rate were investigated, including solution temperature and pH value of solution. The effect of glass structure, defined by the average phosphate anion size and depending on the O/P ratio, on the dissolution behavior will be discussed.

II. $\text{Na}_2\text{O}-\text{CaO}-\text{P}_2\text{O}_5$ Glasses

1. Experimental Procedure

Glasses were melted in Al_2O_3 crucibles at $900\text{--}1200$ °C for one hr, annealed around T_g for four hrs in graphite molds, cut into pieces ($1.0 \times 1.0 \times 0.15$ cm) and polished. Glasses were also crushed into $150\sim 300$ μm powder for some experiments. Polished and powder samples were exposed to different solutions (solution volume/glass surface area = 20); pH value and weight loss were measured at specific time intervals. Solution analyses were done using ICP. Structures were characterized by Raman and XRD.

2. Actual Composition Based on ICP

The volatilization of P_2O_5 from the melts and dissolution of Al_2O_3 into the melts altered the final compositions (Table I).

Table I Difference between batch composition and experimental composition								
Batch Composition				Experimental Composition				Experimental O/P
mol%				mol%				
P ₂ O ₅	Na ₂ O	CaO	O/P	P ₂ O ₅	Na ₂ O	CaO	Al ₂ O ₃	
38	31	31	3.32	35.9	31.6	29.1	3.3	3.48
42	29	29	3.19	38.5	29.3	26.6	5.6	3.45
44	28	28	3.14	41.4	29.3	26.1	3.2	3.29
48	26	26	3.04	45.1	28.3	24.0	2.6	3.17
50	25	25	3.00	48.6	26.5	24.3	0.7	3.04
52	24	24	2.96	49.7	26.2	24.0	0.1	3.01

Looking at glass composition 25Na₂O-25CaO-50P₂O₅ as an example, as melting T increased, the P₂O₅, Na₂O and CaO content of the glass decreases while that of Al₂O₃ increased (Fig. 1),

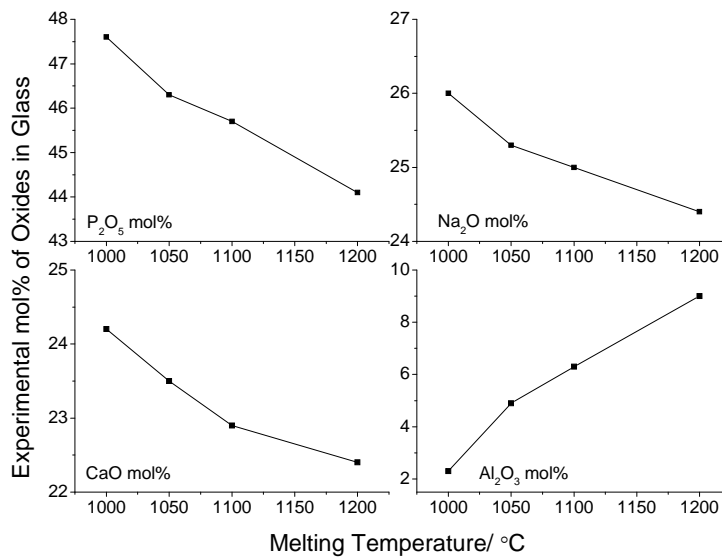


Fig. 1 Effect of melting temperature on the composition of 50P₂O₅ -25Na₂O-25CaO glass.

3. T_g Changed with O/P Ratio of Glasses

T_g temperature of glasses increased first with increasing O/P, and then decreased at higher levels (Fig. 2). The crystallization temperature is 530~650 °C for glasses of O/P 3.01–3.48. In glass composition, the ratio of Na₂O and CaO increased from 1.09 at O/P = 3.01 to 1.17 at O/P = 3.17 and then decreased to 1.09 for glass of O/P = 3.48. But the alumina content of increased as O/P increased to 3.45, and then decreased as O/P increased further to 3.48 (Table I). The apparent trend of T_g vs. temperature may in fact be the effect of Al₂O₃ content, which would be expected to strengthen the glass network.

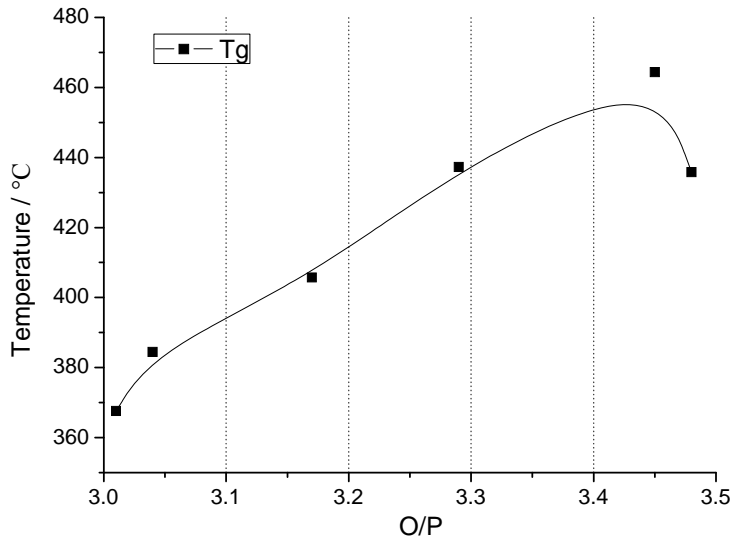


Fig. 2 T_g as an apparent function of O/P ratio of glasses

4. Corrosion Test in Buffer Solutions

The corrosion rate of phosphate glasses is a function of pH. Phosphate glasses with greater O/P ratios dissolved faster in acid (Fig. 3). The O/P ratio at maximum corrosion rate decreased as the pH value of the solution changed from 4 or 10 to 7. Lowest corrosion rates were observed in neutral solutions (Fig. 4).

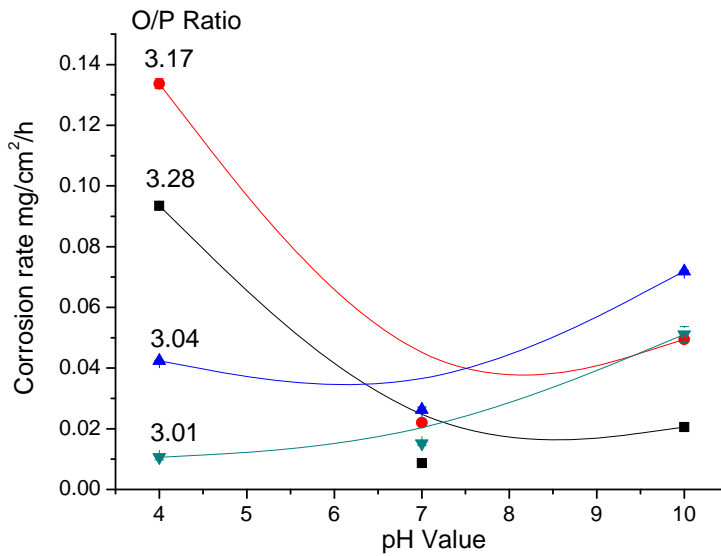


Fig. 3 Corrosion rate of phosphate glass as a function of pH (25 °C, 500 hr)

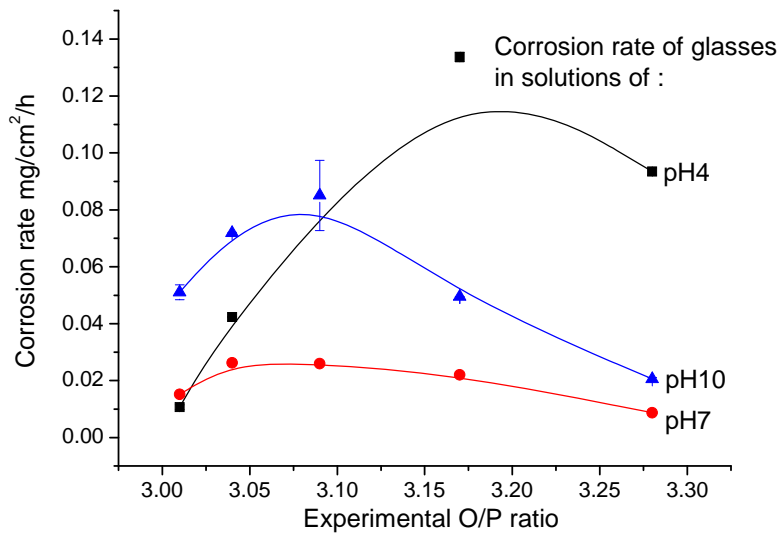


Fig. 4 Corrosion rate of phosphate glass changed with O/P ratio at (25 °C, 500 hr)

Looking at the corroded glass surface and sections of $28\text{Na}_2\text{O}-28\text{CaO}-44\text{P}_2\text{O}_5$ glass in the SEM, there is a layer of precipitation with $0.3\text{--}0.5\ \mu\text{m}$ powder on the glass surface in pH 10 buffer solution after exposure at 25 °C after five months (Fig. 5). This layer could be peeled off easily, exposing new glass surface to the solution. It may be one reason that it was not possible to find the reacted surface through glass sections (Fig. 6). Reacted sections are obvious in glass exposed to the pH 4 buffer solution at 25 °C, which is about $7\text{--}9\ \mu\text{m}$ thick (Fig.7). But for the section from glass exposed to pH 7 buffer solution at 25 °C, it's hard to say whether there is a reaction surface or not (Fig. 8). If there is, the thickness of reacted surface is about $20\ \mu\text{m}$.

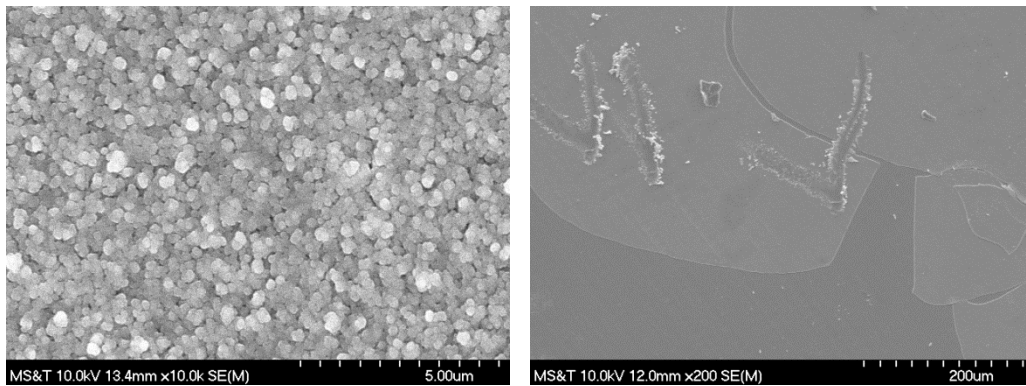


Fig. 5 Reacted surface of $28\text{Na}_2\text{O}-28\text{CaO}-44\text{P}_2\text{O}_5$ glass in pH 10 buffer solution at 25 °C after five months

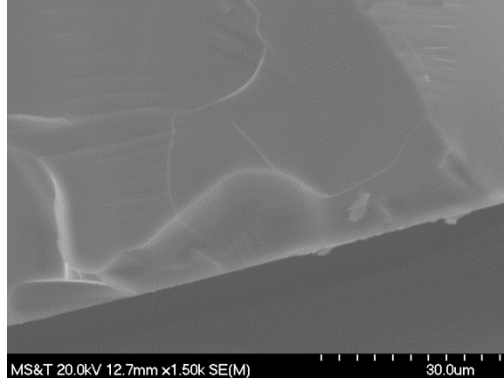


Fig. 6 Reacted section of 28Na₂O-28CaO-44P₂O₅ glass in pH 10 buffer solution at 25 °C after five months

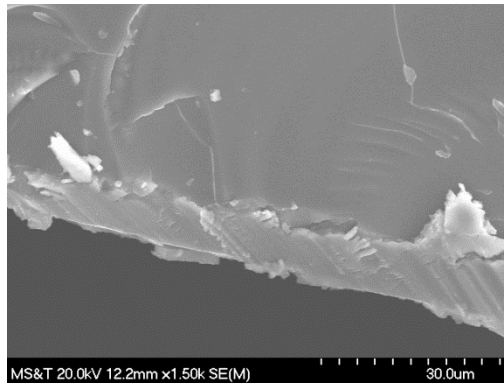


Fig. 7 Reacted section of 28Na₂O-28CaO-44P₂O₅ glass in pH 4 buffer solution at 25 °C after five months

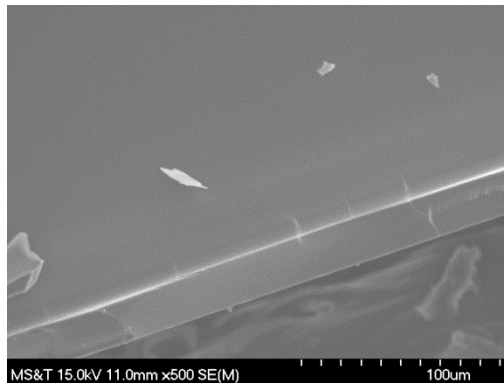


Fig. 8 Reacted section of 28Na₂O-28CaO-44P₂O₅ glass in pH 7 buffer solution at 25 °C after five months

5. Corrosion Test in DI H₂O at 25°C

The dissolution rate of phosphate glasses with O/P = 3.01–3.48 is quite sensitive to glass composition. Corrosion at 25 °C is linear as a function of time except for the glass with O/P = 3.48, which shows $t^{1/2}$ kinetic behavior (Fig. 9). After disassociation of cations from the phosphate

network, hydrolysis of phosphate chains in solution controls solution pH. Glasses with longer chains (lower O/P ratios), form greater concentrations of H_3PO_4 , decreasing pH (Fig. 10).

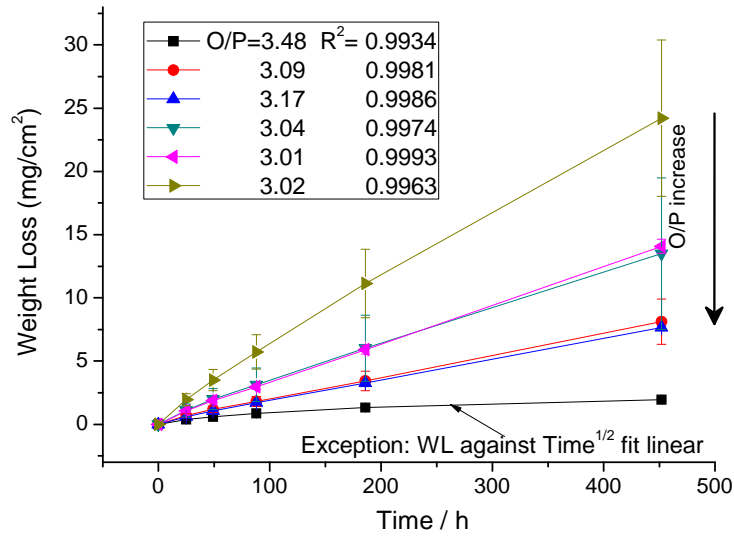


Fig. 9 Corrosion behavior of $Na_2O-CaO-P_2O_5$ glasses in DI H_2O (25 °C, 500 hr)

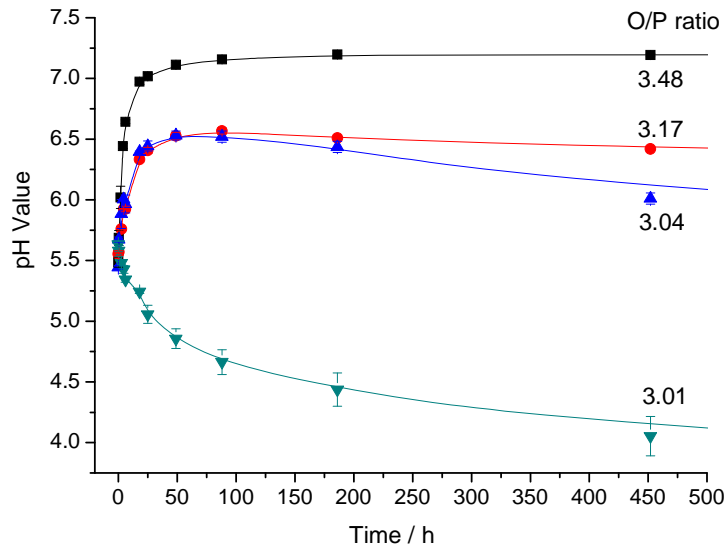


Fig. 10 Change of pH of DI H_2O after exposure to $Na_2O-CaO-P_2O_5$ glasses (25 °C, 500 hrs)

As O/P increases, the glass corrosion rate decreases (Fig. 11). The corrosion products on the glass surface after 2340 hrs are an amorphous phosphate phase (Fig. 12). The corrosion rates of different compositions after 2340 hr are listed in Table II.

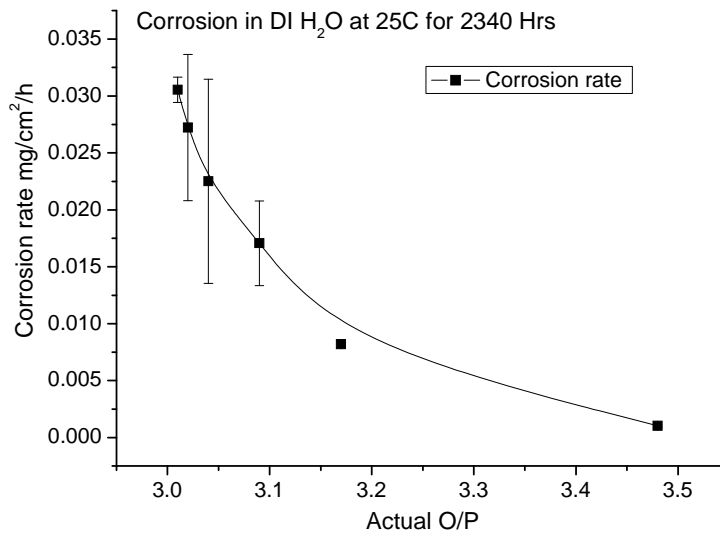


Fig. 11 Corrosion rate of Na₂O-CaO-P₂O₅ glass as a function of O/P ratio (DI H₂O, 25 °C for 2340 hrs)

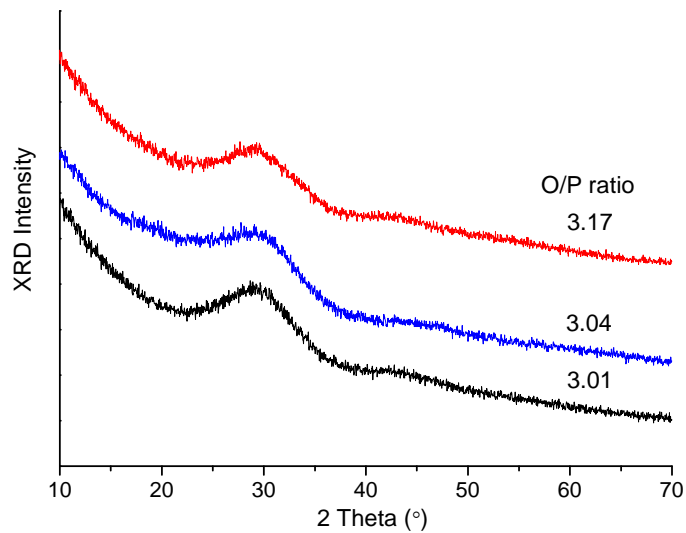


Fig. 12 XRD of the surface of corroded Na₂O-CaO-P₂O₅ glass (DI H₂O, 25 °C, 2340 hr)

6. Corrosion Test in DI H₂O at 60 °C

Weight loss of bulk glasses in DI water at 60 °C are much faster than that at 25 °C, and do not exhibit a linear time dependence (Fig. 13). The changes of pH are shown in Fig. 14. After 168 hrs in DI H₂O at 60 °C, there are layers of precipitation on the glass surface at O/P = 3.04–3.29 (Fig. 15), and for the glass of O/P = 3.04, the glass showed porous structure (Fig. 16). And as O/P decreased, so did the thickness of the precipitation layer. XRD analysis showed that the precipitation is an amorphous phosphate corrosion product (Fig. 17).

Table II Corrosion rate of different compositions at 25 °C for 452 and 2340 hr

Actual O/P	Solubility (g/cm ² /min) / 10 ⁻⁷			
	452 Hrs		2340 Hrs	
	AVE	SD	AVE	SD
3.48	0.72	0.03	0.17	0.02
3.17	2.82	0.04	1.37	0.05
3.09	2.99	0.66	2.84	0.62
3.04	4.98	2.21	3.75	1.50
3.02	8.93	2.28	4.54	1.07
3.01	5.19	0.20	5.09	0.19

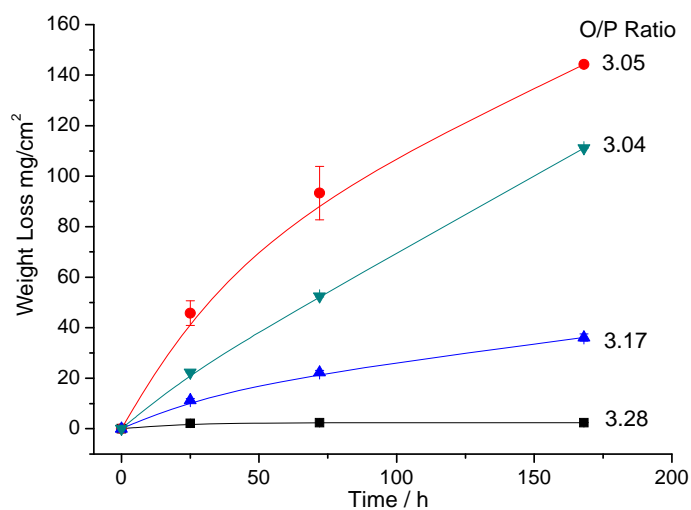


Fig. 13 Weight loss of Na₂O-CaO-P₂O₅ glass at 60 °C (DI H₂O, 168 hr)

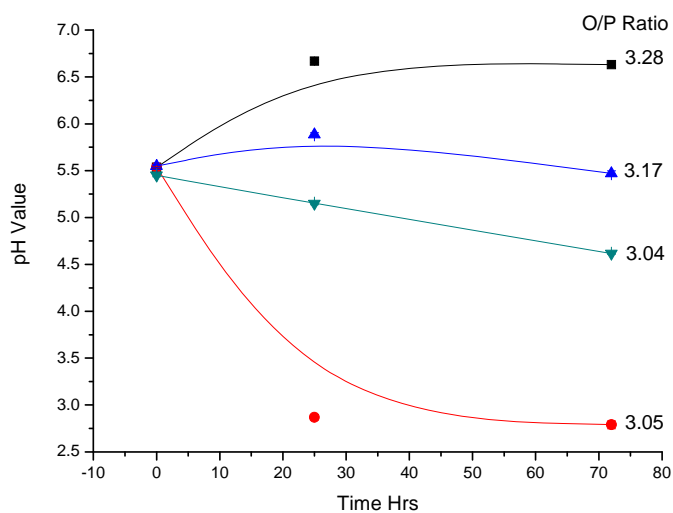


Fig. 14 pH shift of Na₂O-CaO-P₂O₅ glass at 60 °C (DI H₂O, 72 hr)

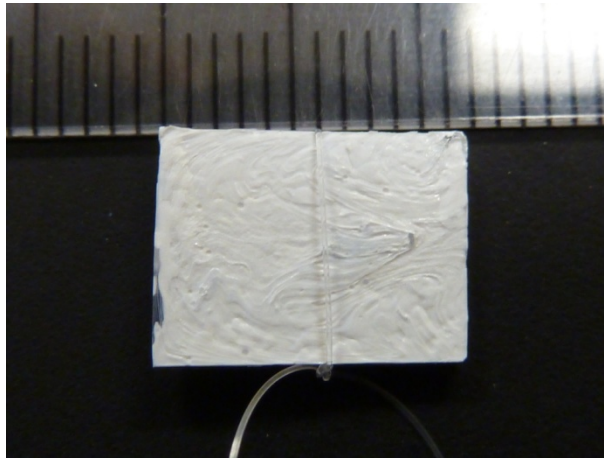


Fig. 15 Porous structure of Na₂O-CaO-P₂O₅ glass (O/P = 3.17) after 168 Hrs

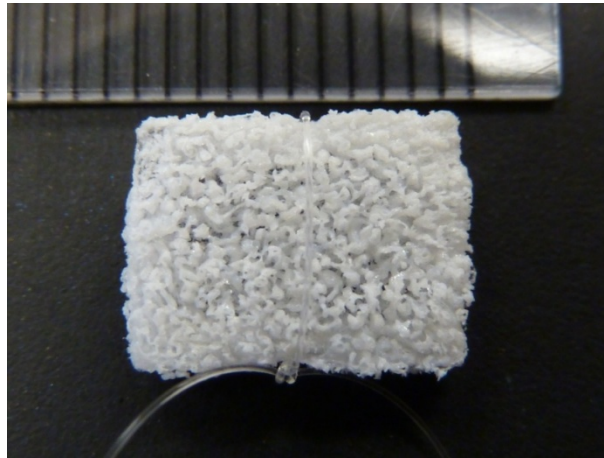


Fig. 16 Porous structure of Na₂O-CaO-P₂O₅ glass (O/P = 3.04) after 168 Hrs

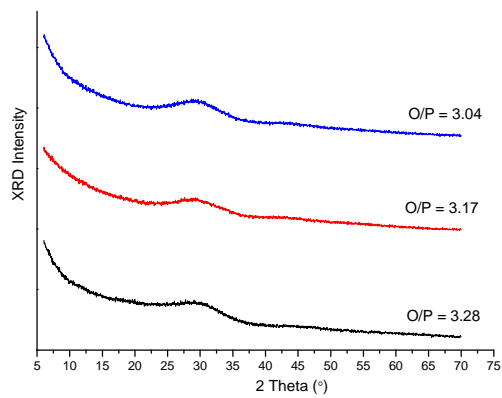


Fig. 17 Amorphous phosphate corrosion product (168 hr)

FTIR absorption band assignments are shown in Table III. The bands in the 650~665 cm⁻¹ region may be assigned to the bending vibration of bridging phosphorus, $\delta(\text{O-P-O})$ and/or $\delta(\text{P=O})$ units. Corrosion in water led to a substantial breakdown of P=O and O-P-O bonds in the glass network, and the bands shifted towards 675~690 cm⁻¹, with decreased intensity. The average length of phosphate chain structures decreased under H₂O attack (Fig. 18).

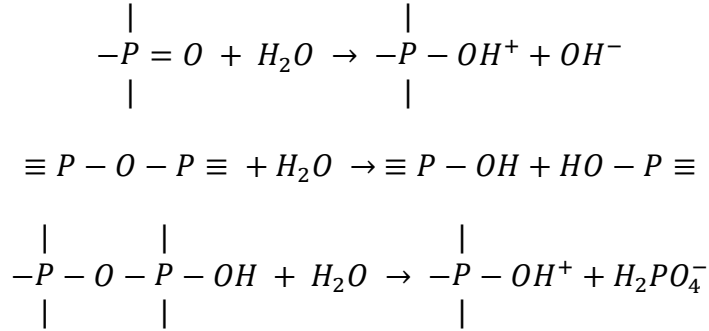
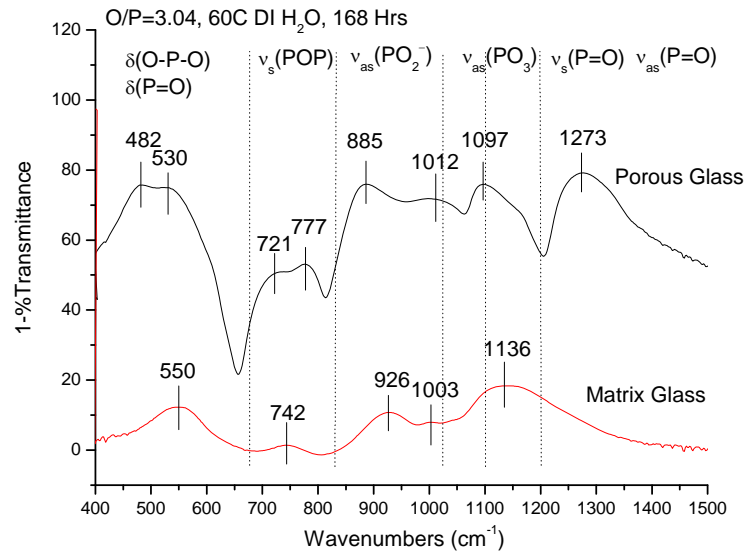


Table III FTIR absorption bands assignment for studied phosphate*

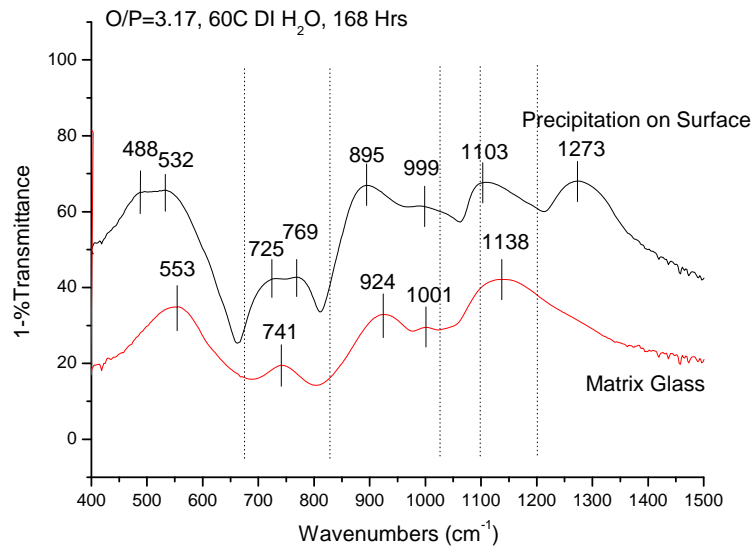
Wavenumber (cm ⁻¹)		Wavenumber (cm ⁻¹)	
458-680	Bending vibrations of bridging phosphorus $\delta(\text{O-P-O})$ and/or $\delta(\text{P=O})$	472	O-P-O bending (CaHPO ₄)
		498	symmetrical terminal P-O bending mode $\delta_s\text{PO}_3$ (CaP)
		528	$\delta_s\text{PO}_3, \delta_{as}\text{PO}_3$ ($\beta\text{-Ca}_2\text{P}_2\text{O}_7$)
		536	asymmetrical terminal P-O bending mode $\delta_{as}\text{PO}_3$
		567	$\delta_{as}\text{PO}_3$
		583	O-P-O(H) bending (CaHPO ₄)
		585	$\delta_s\text{PO}_3$ ($\gamma\text{-Ca}_2\text{P}_2\text{O}_7$)
715-830	Symmetric stretch of P-O-P bridges, $\nu_s\text{POP}$	720	$\nu_s\text{POP}$ ($\gamma\text{-Ca}_2\text{P}_2\text{O}_7$)
880-1022	Asymmetric stretch of (P-O-P) bridges in metaphosphate configurations (Q ₂), $\nu_{as}(\text{PO}_2^-)$	892	P-O(H) stretching(CaHPO ₄)
		954	asymmetrical bridge P-O-P stretching mode $\nu_{as}\text{POP}$ ($\gamma\text{-Ca}_2\text{P}_2\text{O}_7$)
		995	P-O symmetric stretching (CaHPO ₄)
		1001	symmetrical terminal P-O stretching mode $\nu_s\text{PO}_3$ ($\gamma\text{-Ca}_2\text{P}_2\text{O}_7$)
~1100	Asymmetric stretch of (P-O-P) bridges in pyrophosphate groups (Q ₁), $\nu_{as}(\text{PO}_3^{2-})$		
1080-1170	$\nu_{as}\text{PO}_3$ asymmetrical terminal P-O stretching mode	1087	$\nu_{as}\text{PO}_3$ ($\gamma\text{-Ca}_2\text{P}_2\text{O}_7$)
		1144	$\nu_{as}\text{PO}_3$ ($\gamma\text{-Ca}_2\text{P}_2\text{O}_7$)
		1165	$\nu_{as}\text{PO}_3$ ($\gamma\text{-Ca}_2\text{P}_2\text{O}_7$)
~1200	Symmetric stretch of (P=O) bonds, $\nu_s(\text{P=O})$		
1260-1340	Asymmetric stretch of (P=O) bonds, $\nu_{as}(\text{P=O})$		

* Y.M. Moustafa, K. El-Egili. Infrared spectra of sodium phosphate glasses. Journal of Non-Crystalline Solids 240 (1998) 144-153.

* C. Q. Ning, Y. Greish, A. El-Ghannam. Crystallization behavior of silica-calcium phosphate biocomposites: XRD and FTIR studies. Journal of Materials Science: Materials in Medicine 15, (2004) 1227-1235.



(a)



(b)

Fig. 18 IR spectroscopy of corroded glasses with O/P = 3.04 (a) and 3.17 (b) (DI H₂O, 60 °C)

7. Ion concentrations in Solutions

Long term corrosion tests show different dissolution behavior. Ion release rates depend on O/P ratio, for low-to mid O/P (3.01–3.09), essentially linear release rates with time for all ions; for high O/P (3.17-3.48), the downward concave curve suggests that leaching rate of ions slowed with time (Fig. 19).

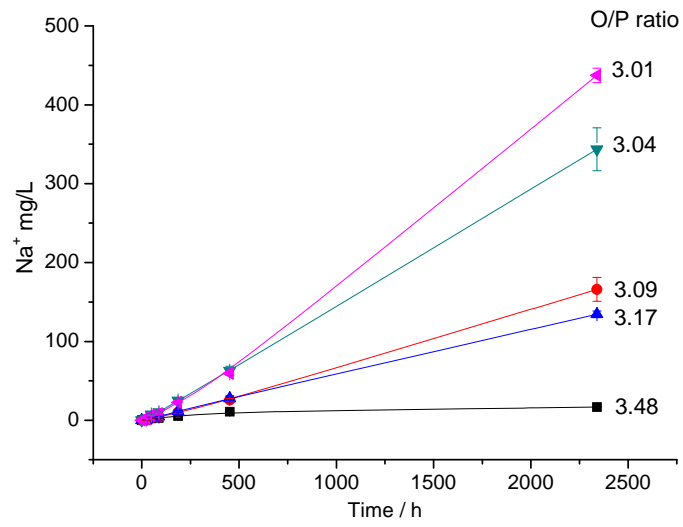
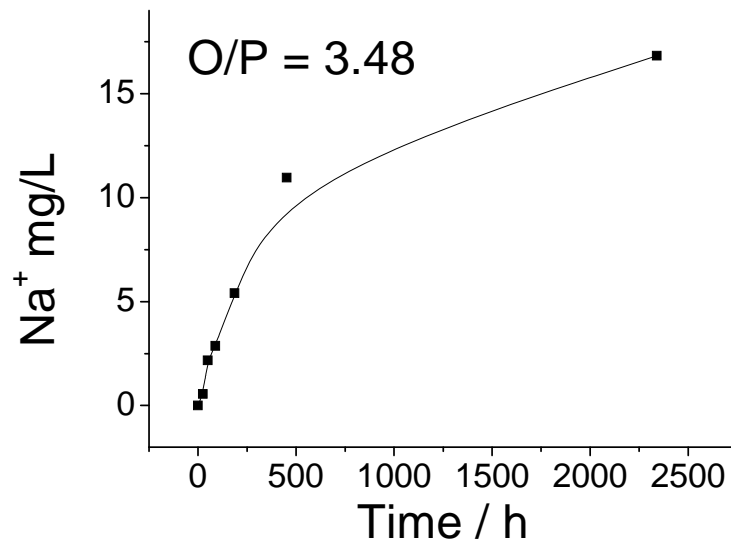


Fig. 19 (a)



(b)

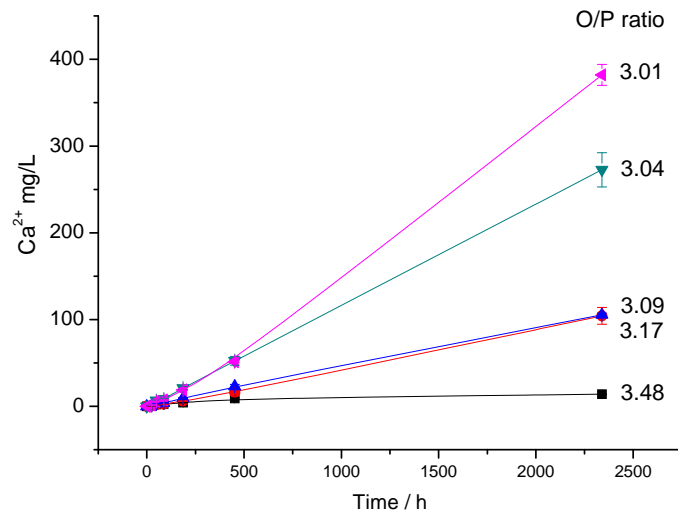
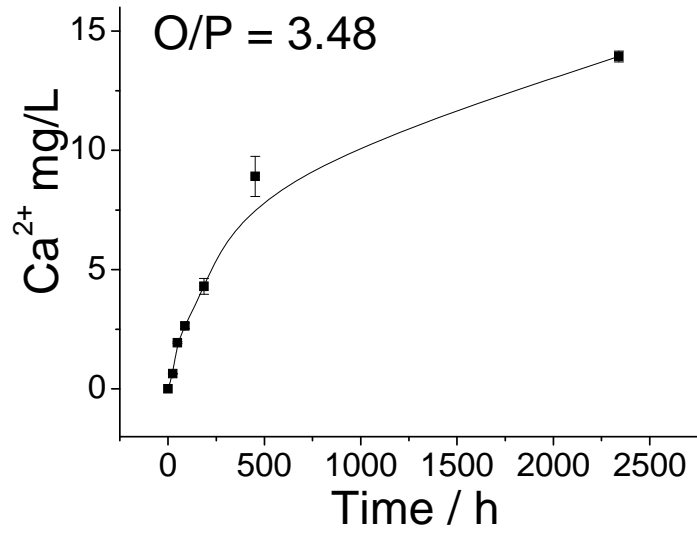
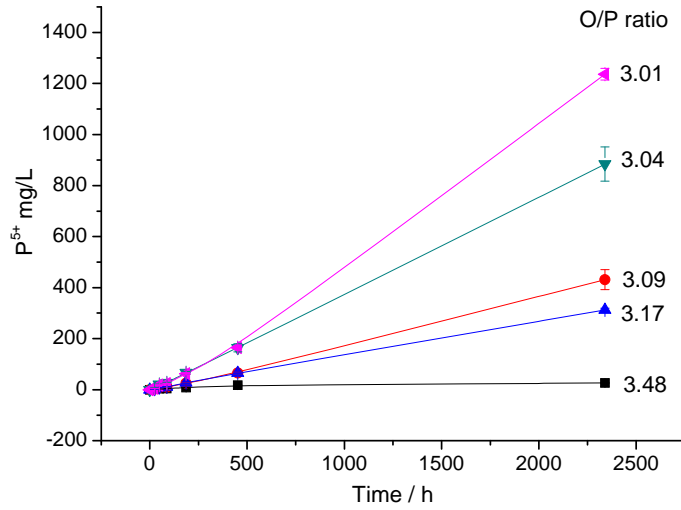


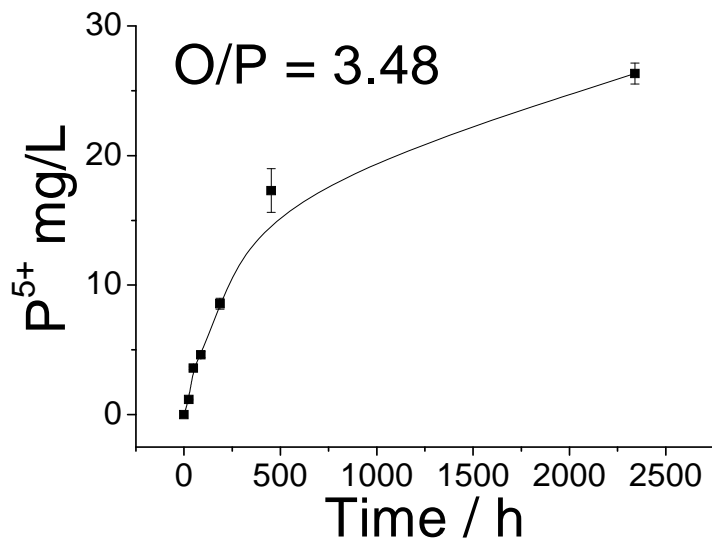
Fig. 19(c)



(d)



(e)



(f)

Fig. 19(a-f) Ion release rates from $\text{Na}_2\text{O-CaO-P}_2\text{O}_5$ glass in long term corrosion tests

Ion concentrations in solution are similar to those in the original glasses, indicating that the glasses dissolve congruently (Fig. 20). Solutions at specific time were analyzed by ICP and the compositions of glass dissolved into H_2O were calculated (Table IV). The differences between glass matrix and glass dissolved into H_2O are shown in Table V. Phosphate glasses appear to dissolve uniformly in DI H_2O and the weight-loss measurements match well with ICP results.

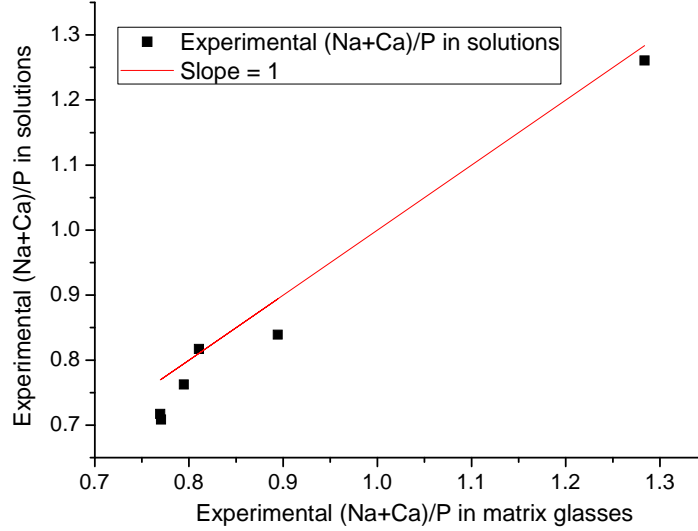


Fig. 20 Comparison of (Na/Ca)/P ratio in matrix glasses with that in solution

Batch Composition				Experimental Composition				Glass Dissolved in Solution			
mol%				mol%				mol%			
P ₂ O ₅	Na ₂ O	CaO	O/P	P ₂ O ₅	Na ₂ O	CaO	O/P	P ₂ O ₅	Na ₂ O	CaO	O/P
38	31	31	3.32	37.2	32.7	30.1	3.35	37.4	31.7	30.9	3.94
40	30	30	3.25	49.6	30.0	20.4	3.01	49.5	30.3	20.3	3.07
45	28	28	3.11	50.1	27.3	22.6	3.00	52.7	27.4	19.9	3.09
48	26	26	3.04	46.3	29.1	24.6	3.06	47.6	27.4	25.1	3.10
50	25	25	3.00	48.9	26.6	24.5	3.02	49.9	26.0	24.1	3.03
52	24	24	2.96	49.7	26.2	24.1	3.01	51.1	24.4	24.5	3.04

Experimental O/P	Difference between Glass Matrix and Glass Dissolved in DI H ₂ O/ %							Different between Glass Dissolved in H ₂ O and Weight Loss/ %
	O/P	P ₂ O ₅	Na ₂ O	CaO	Na/P	Ca/P	Na/Ca	
3.35	17.61	0.54	-3.06	2.66	-3.58	2.11	-5.57	7.60
3.06	1.31	2.81	-5.84	2.03	-8.41	-0.75	-7.72	0.87
3.02	0.33	2.05	-2.26	-1.63	-4.21	-3.60	-0.63	0.38
3.01	1.99	-0.20	1.00	-0.49	1.20	-0.29	1.50	0.95
3.01	1.00	2.82	-6.87	1.66	-9.42	-1.13	-8.39	0.94
2.96	3.00	5.19	0.37	-11.95	-4.59	-16.29	13.98	2.51

Fitting amount of dissolved glass vs. time into product layer diffusion model controlled by surface reaction (Fig. 21).

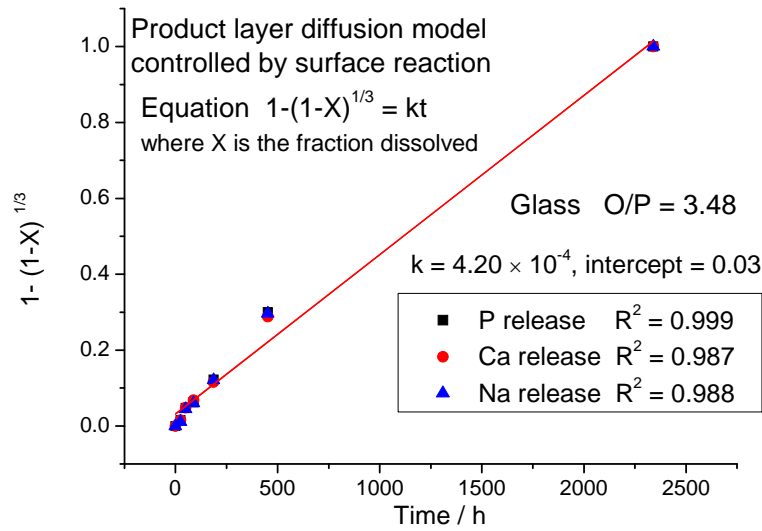


Fig. 21 Product layer diffusion model

Similar Raman spectra were collected from base glasses and their surfaces after 2340 hrs of corrosion in DI water (Fig. 22). Morphologies of glass surfaces are shown in Fig. 23.

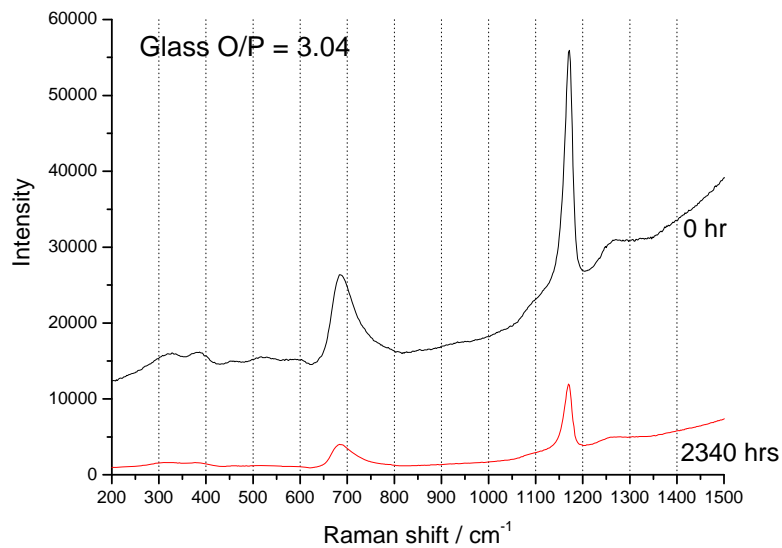


Fig. 22 Raman spectra are collected from base glasses and their surfaces after 2340 hrs

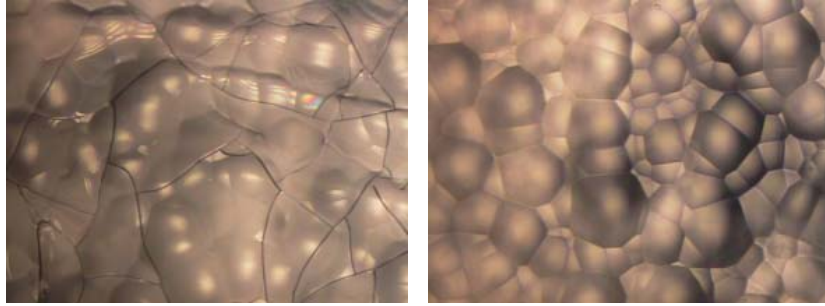


Fig. 23 Morphology of glass surface after 2340 hrs in DI H₂O taken by optical microscope (10X)

8. Summary

The dissolution behavior of Na/Ca-phosphate glasses with O/P = 3.01~ 3.48 is sensitive to solution pH and glass composition. Dissolution kinetics of phosphate glasses in DI H₂O are dependent on corrosion time and temperature. Glasses dissolve congruently, although the time dependence varies between linear and $t^{1/2}$ kinetics. Ion release rates exhibit different dissolution behavior in long term corrosion tests and depend on O/P ratio of matrix glasses.

III. Na₂O-Fe₂O₃-P₂O₅ Glasses

1. Experimental Procedure

Glasses were melted in SiO₂ and Al₂O₃ crucibles at 1100~1250 °C for two hr, annealed around T_g for 4 hrs, cut into pieces (1.0 × 1.0 × 0.15 cm) and polished. Glasses were also crushed into 150–300 μm and 300–425 μm powder for some experiments. Polished and powder samples were exposed to different solutions (solution volume/glass surface area = 20); pH value and weight loss were measured at specific time intervals. Solution analyses were done using ICP. Structures were characterized by Raman and XRD.

2. Glass Melting

Fe-P glasses were melted in fused SiO₂ crucibles (Leco 728-701) at 1050~1250 °C for two hr. The melts were poured onto a copper plate and quenched by pressing another cold copper plate to room temperature.

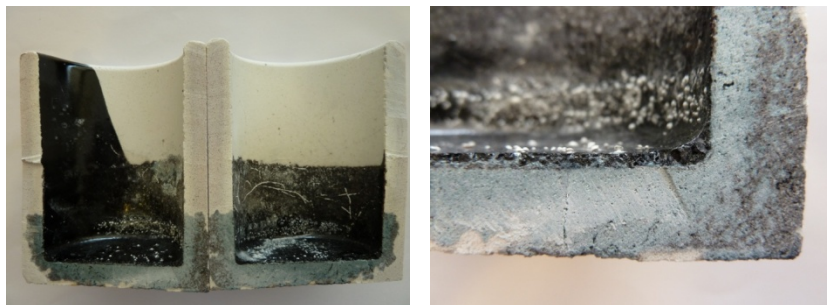


Fig. 24 SiO₂ crucible after melting NFP-3.5-40 glass

Table VI Batched Composition and Measured Density							
O/P	Code	Fe/P	Glasses mol%			Density g/cm ³	
			Na ₂ O	Fe ₂ O ₃	P ₂ O ₅	Ave	Std
3.0	NFP-3.0-25	0.33	0	25	75	2.743	0.031
	NFP-3.0-15	0.23	20	15	65	2.671	0.006
3.25	NFP-3.25-33.3	0.5	0	33.3	66.67	2.841	0.003
	NFP-3.25-17.78	0.33	28	17.78	54.22	2.815	0.005
	NFP-3.25-11.11	0.23	40	11.11	48.89	2.723	0.010
3.5	NFP-3.5-40	0.67	0	40	60	2.954	0.003
	NFP-3.5-14.2	0.33	43	14.2	42.8	2.815	0.001
	NFP-3.5-9.1	0.23	51.5	9.1	39.4	2.721	0.007

The penetration of glasses into SiO₂ crucibles was very severe for some compositions (Fig. 24). While melting the same glass in Al₂O₃ crucible, there is no such problem (Fig. 25).

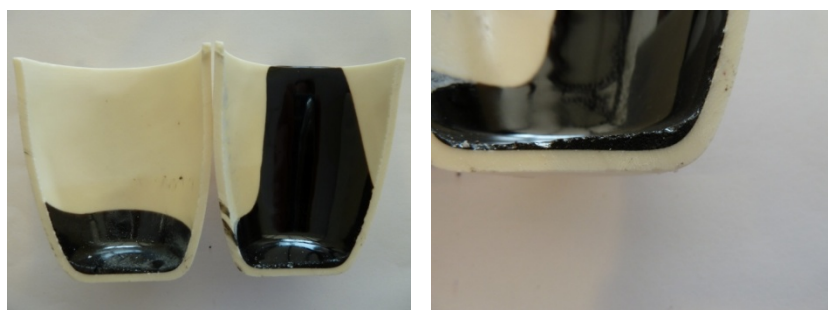


Fig. 25 Al₂O₃ crucible after melting NFP-3.5-40 glass

3. Glass Digestion

Experimental O/P ratio was calculated from the percentages in the glass of Fe₂O₃, Na₂O, P₂O₅, SiO₂, and Al₂O₃ (Table VII). Actually, Fe²⁺ and Fe³⁺ co-existing in the glass network would change these ratios. However, glass digestion which could be used for titration of relative Fe²⁺/Fe³⁺ ratio was not successfully performed. As a result, the actual ratio of Fe²⁺ to Fe³⁺ is unknown.

The Fe/P ratio in the melted glass is close to the ratio as batched. But the O/P ratio changed considerably, possibly due to valence change of Fe and/or volatilization of P. If the Fe²⁺/Fe³⁺ ratio was known, the calculated O/P ratio in the melted glasses would be more accurate.

Except for batched Na-free glasses, which acquired Na contamination from the crucibles, all the other glasses lost large amount of Na during melting. But P₂O₅ content increased in the experimental composition. The unknown Fe²⁺/Fe³⁺ ratio affects these calculations considerably. As a result, the actual Na lost may not be so great.

Table VII Batch composition and experimental composition

Batch Composition (wt.-%)					Experimental Composition (wt.-%)						
O/P	Fe ₂ O ₃	Na ₂ O	P ₂ O ₅	Fe/P	O/P*	Fe ₂ O ₃	Na ₂ O	P ₂ O ₅	SiO ₂	Al ₂ O ₃	Fe/P
3.5	40	0	60	0.67	3.47	38.16	0.13	60.37	1.23	0.11	0.63
3.5	14.2	43	42.8	0.33	3.24	19.25	21.35	56.87	2.44	0.08	0.34
3.5	9.1	51.5	39.4	0.23	3.31	12.32	26.1	53.34	1.56	6.68	0.23
3.25	33.3	0	66.67	0.5	3.29	31.69	0.37	64.78	3.17	0	0.49
3.25	17.78	28	54.22	0.33	3.12	21.21	12.39	64.43	1.97	0	0.33
3.25	11.11	40	48.89	0.23	3.07	14.98	18.64	62.66	3.68	0.03	0.24
3	25	0	75	0.33	3.12	25.09	0.26	69.5	5.16	0	0.36
3	15	20	65	0.23	2.96	16.87	8.58	71.14	3.41	0	0.24

4. PCT Test

The PCT was conducted following the procedures of ASTM C 1285-97. The glass powder (-100 +200 mesh) was ultrasonically washed with absolute ethanol to remove dust particles before mixing with DI H₂O in a Teflon vessel. Duplicate samples were kept at 90±2 °C for seven days. The concentrations of ions in the leachant were measured by ICP-OES (Table VIII).

Table VIII ICP-OES Results of PCT Leachant

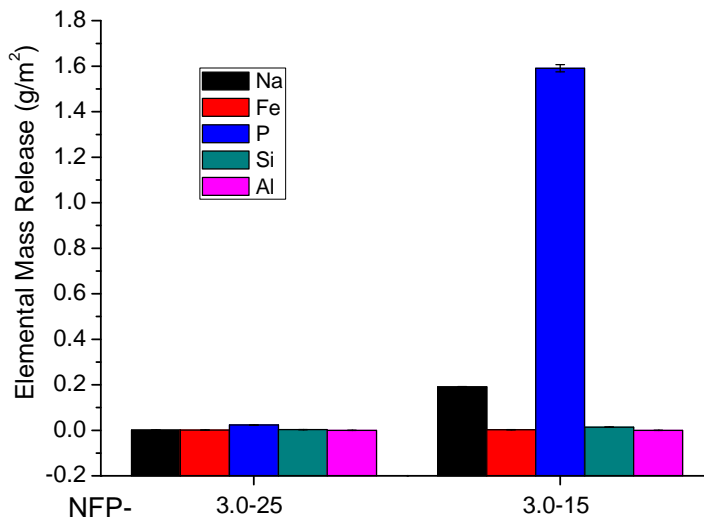
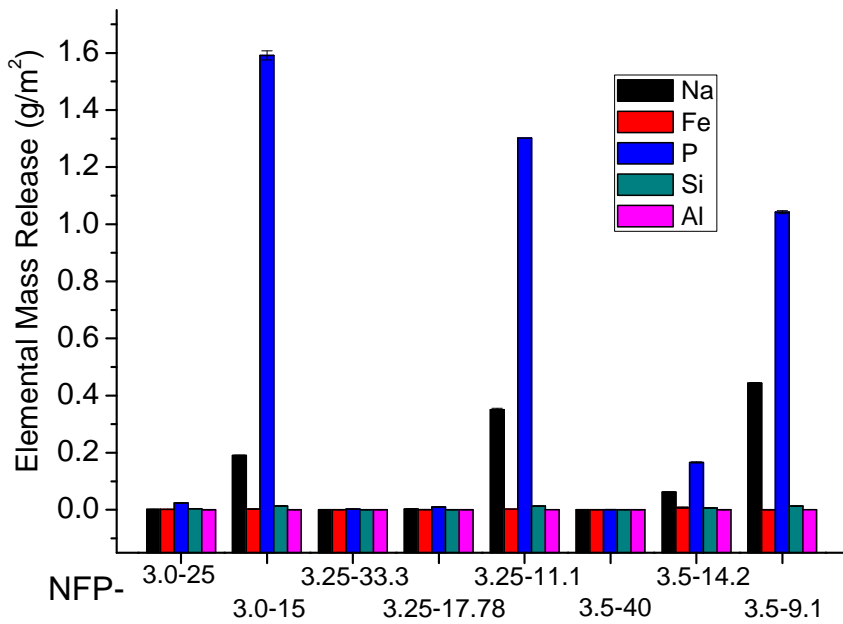
Code (NFP-)	Na / ppm		Fe / ppm		P / ppm		Si / ppm		Al / ppm		pH After PCT
	Ave	Std	Ave	Std	Ave	Std	Ave	Std	Ave	Std	
3.0-25	19.98	0.50	16.95	1.63	321.25	6.75	50.20	1.2	0.1	0.1	2.15
3.0-15	2610.0	14.1	37.00	5.66	21750.0	212.	189.0	9.9	4.0	1.4	1.73
3.25-33.3	0.96	0.57	6.72	0.06	41.18	0.64	3.31	0.2	0.1	0.0	2.56
3.25-17.78	42.23	1.23	14.15	2.43	136.25	3.30	5.70	0.3	0.1	0.1	5.42
3.25-11.1	4790.0	70.7	30.0	0.00	17800.0	0.00	176.0	2.8	3.0	0.0	3.26
3.5-40	1.06	0.50	0.17	0.17	14.20	0.47	1.47	0.2	0.0	0.1	3.73
3.5-14.2	857.75	13.9	109.4	30.78	2275.00	19.15	91.18	2.21	1.43	1.31	6.43
3.5-9.1	6065.00	21.21	3.50	0.71	14250.00	70.71	180.50	4.95	2.00	0.00	6.63

According to ASTM C 1285-02 (2008), a normalized elemental release rate, NR_i, was calculated from Eq. (1):

$$R_i (\text{g} / \text{day} - \text{m}^2) = \frac{C_i}{f_i \frac{SA}{V} t} \quad (1)$$

C_i is the concentration of element i in the solution ($\text{g/m}^3 = \text{ppm} = \text{mg/l}$) and f_i is the mass fraction of element i in the unleached glass (unitless), which is calculated using the analyzed glass composition given in Table VII. SA/V is the ratio of the sample surface area to volume of leachate (m^{-1}). A value of 1953 m^{-1} for SA/V as calculated per the procedures in ASTM C 1285-97 was used for all samples.

Figure 26 is the unnormalized elemental release ($\text{g/m}^2\text{-day}$) from Fe-P glasses after PCT in DI H_2O at 90°C for seven days. Since the exact glass composition is currently unknown, the mass fraction of element i in the unleached glass is unknown.



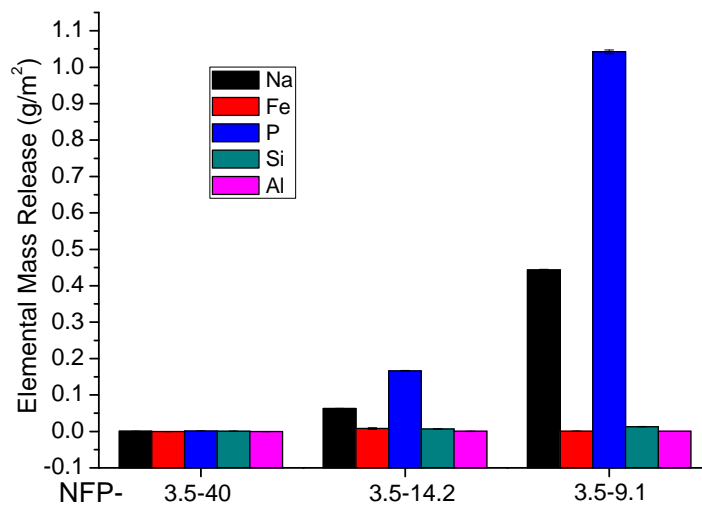
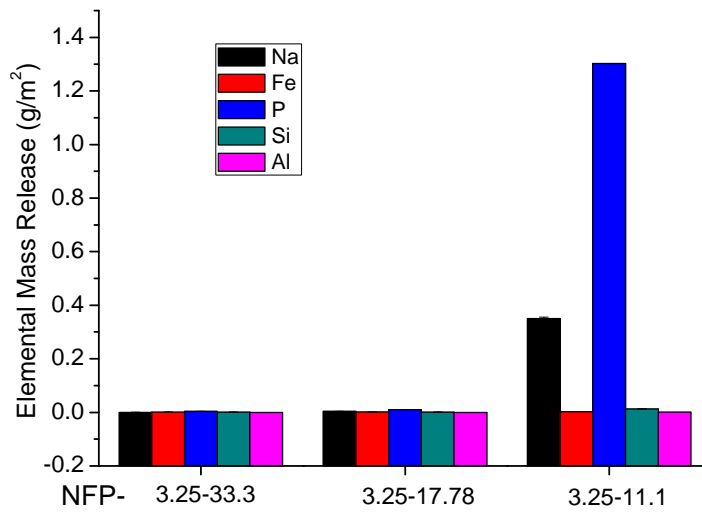
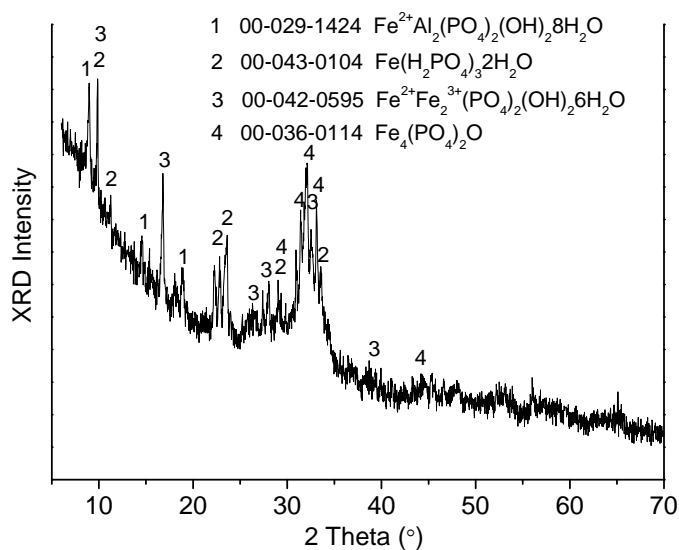


Fig. 26 (a-d) Elemental release ($\text{g}/\text{m}^2\text{-day}$) from Fe-P glasses after PCT in DI H_2O at 90°C for seven days

5. Raman and XRD Spectra of Fe-P Glass after PCT

After the PCT test, some glasses has crystallized. The leaching test resulted not only in elemental dissolution, but precipitation and crystallization as well. Figures 27–29 are the Raman and XRD spectra of some Fe-P glasses after the PCT test.



XRD Spectra of NFP-3.5-9.1 Dry PCT Powder

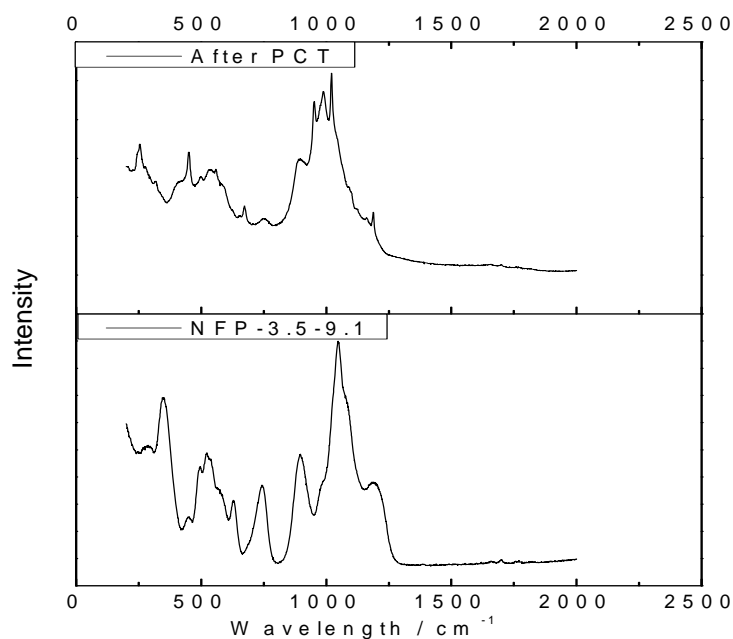
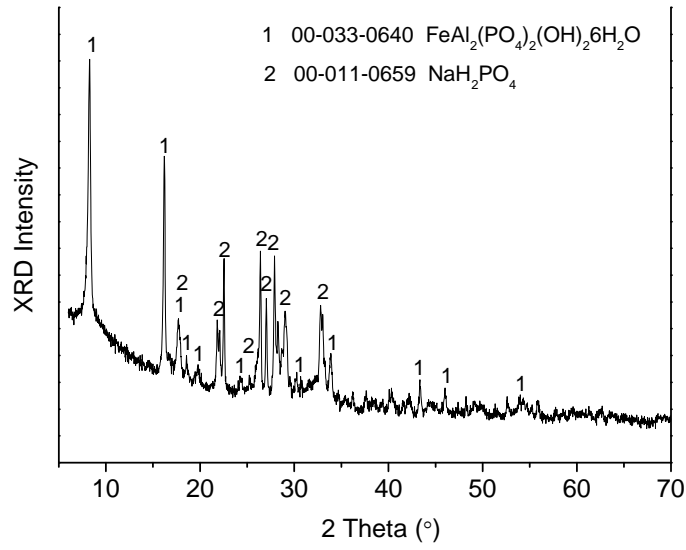


Fig. 27 NFP-3.5-9.1 Glasses after PCT test



XRD Spectra of NFP-3.25-11.1 Dry PCT Powder

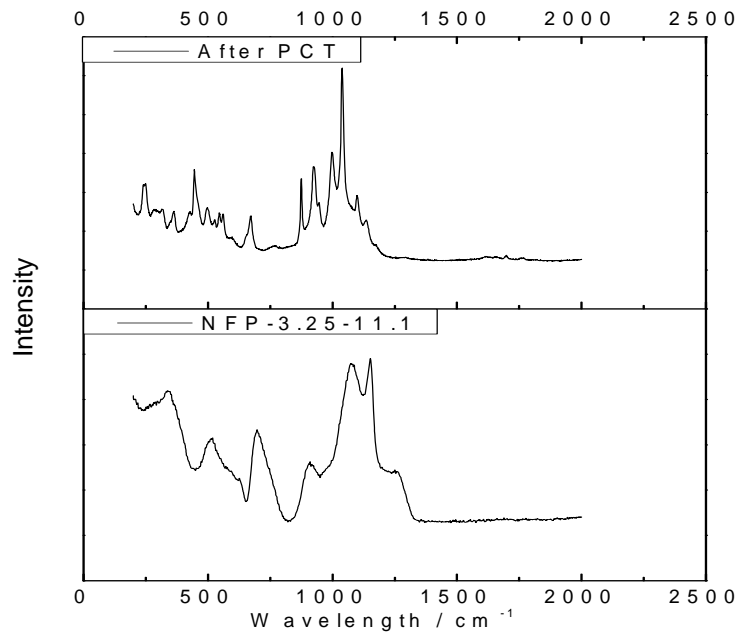
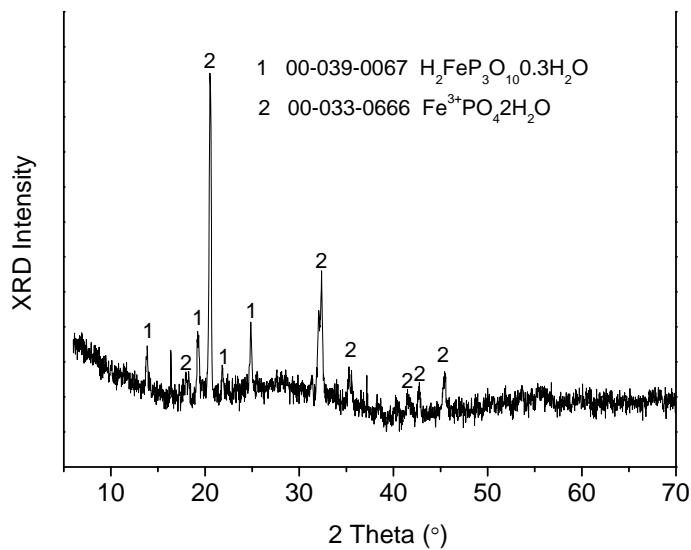


Fig. 28 NFP-3.25-11.1 Glasses after PCT test



XRD Spectra of NFP-3.0-15 Dry PCT Powder

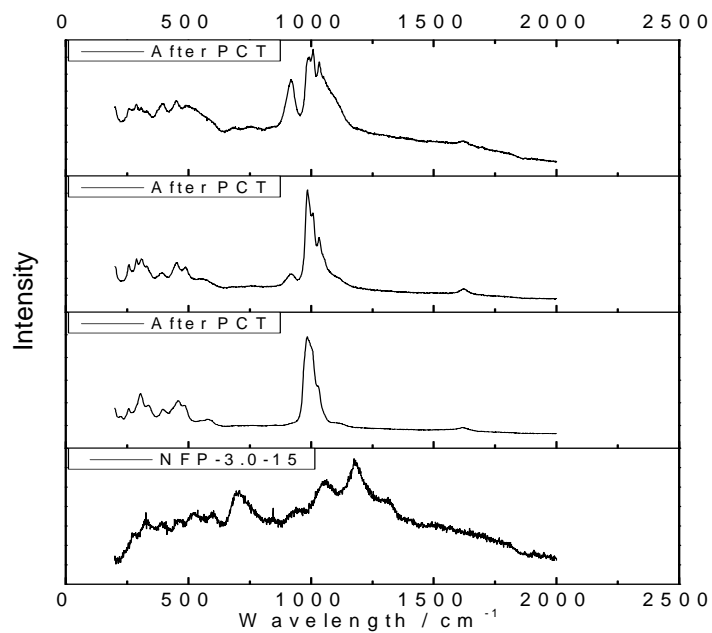


Fig. 29 NFP-3.0-15 Glasses after PCT test

6. Dissolution Rate of Fe-P Glasses

Glass powders (150–355 μm and 355–425 μm) were ultrasonically washed with absolute ethanol to remove dust particles, and then sealed into small bags (2 \times 2 cm) made with Nylon mesh (284 TPI mesh, opening size of 51 μm , and an open area of 32 percent). Prepared samples were held in DI H₂O at room temperature (25 °C) for 350 hrs, weight loss and pH values were measured every specific time. The dissolution rate (D_R) was calculated from the measured weight loss per units surface area. The pH value of the solution changed over time due to the dissolution of the glasses. The pH value of DI H₂O is 5.787 at room temperature. Figure 30 is the dissolution rate of Fe-P glass in DI H₂O at room temp.,

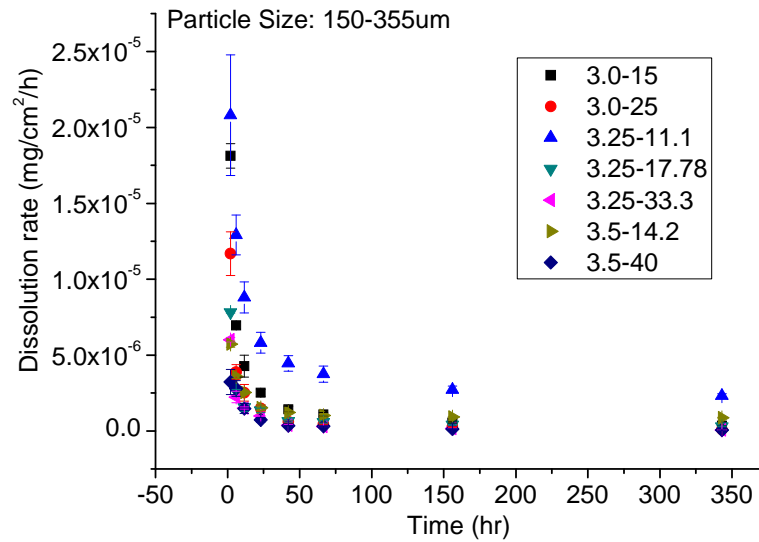
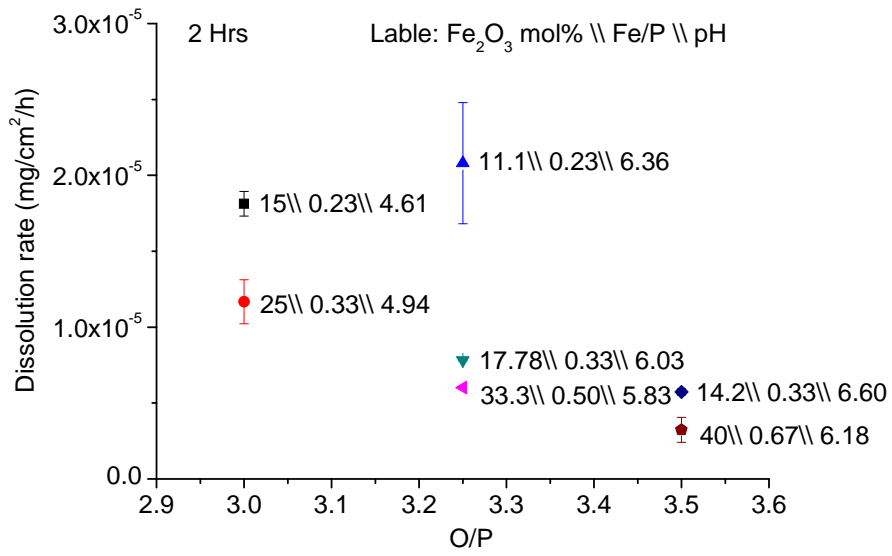
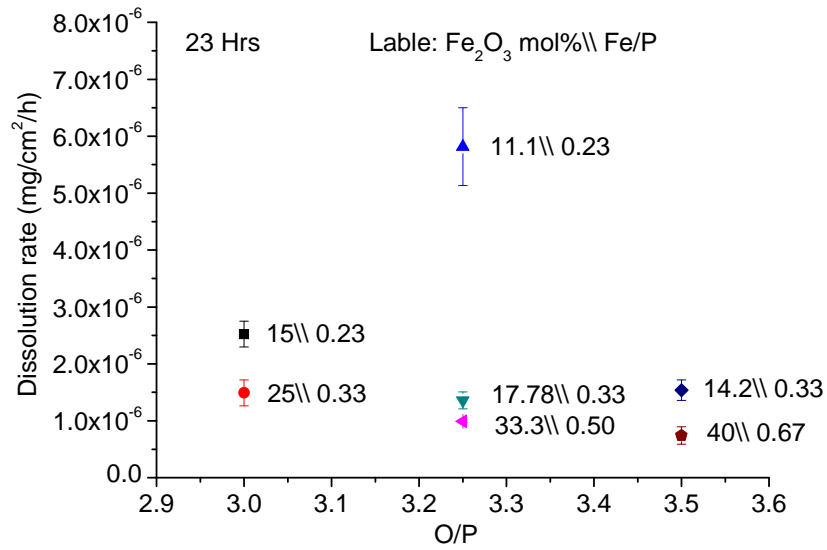


Fig. 30 Dissolution rate of Fe-P glass in DI H₂O at room temperature

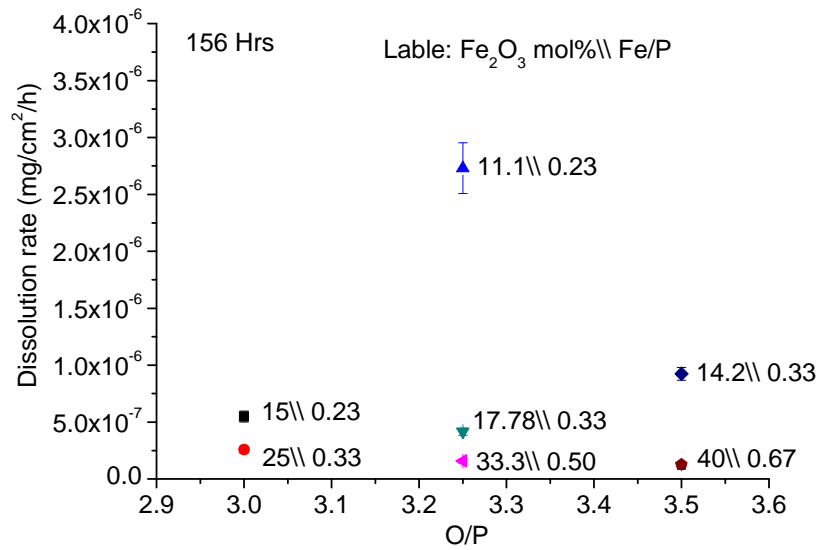
For specific testing times, the dissolution rate was affected by both O/P and Fe/P of tested glass. Figure 31 shows how D_R of glass powder (150–355 μm) changed with O/P and Fe/P. Since the actual composition of glasses wasn't completely analyzed, conclusions are based on the as-batched compositions: 1. higher Fe/P = lower dissolution rate; 2. higher O/P = lower dissolution rate for short-time exposure; 3. same Fe/P, lower O/P = lower dissolution rates after longer leaching times.



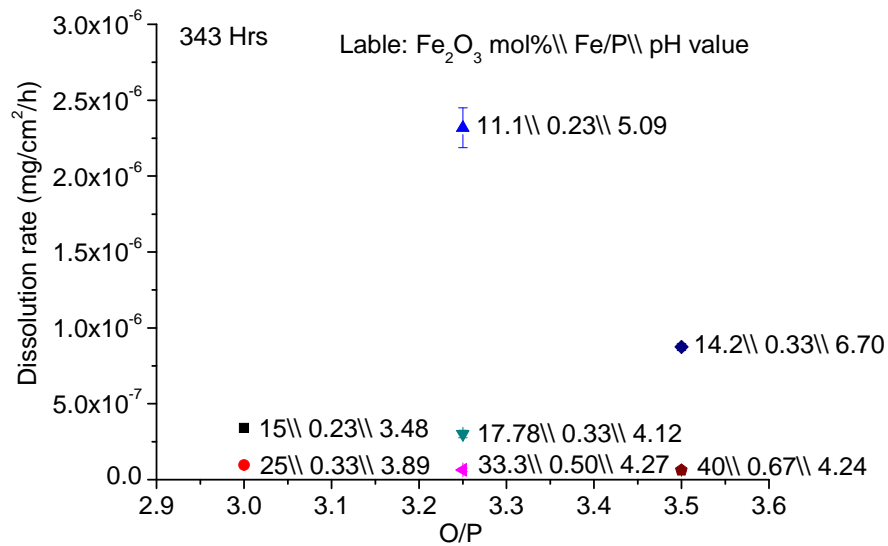
(a) D_R (mg/cm²-h) for two hr test



(b) D_R (mg/cm²-h) for 23 hr test



(c) D_R (mg/cm²-h) for 156 hr test



(d) D_R (mg/cm²-h) for 343 hr test

Fig. 31(a-d) D_R of glass powder (150–355 μ m) affected by O/P and Fe/P

The effects of glass particle size on dissolution rate are not obvious except for NFP-3.5-9.1. Figure 32 shows how the D_R of glass with O/P = 3.5 changed with particle size and time. Figure 33 is the D_R of glass with O/P = 3.25 for varying particle size and time. Figure 34 is the D_R of glass with O/P = 3.0 changed with particle size and time.

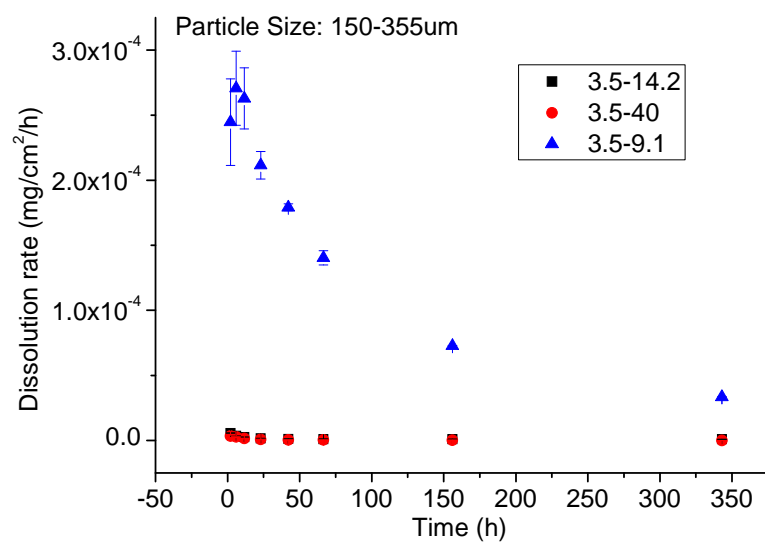
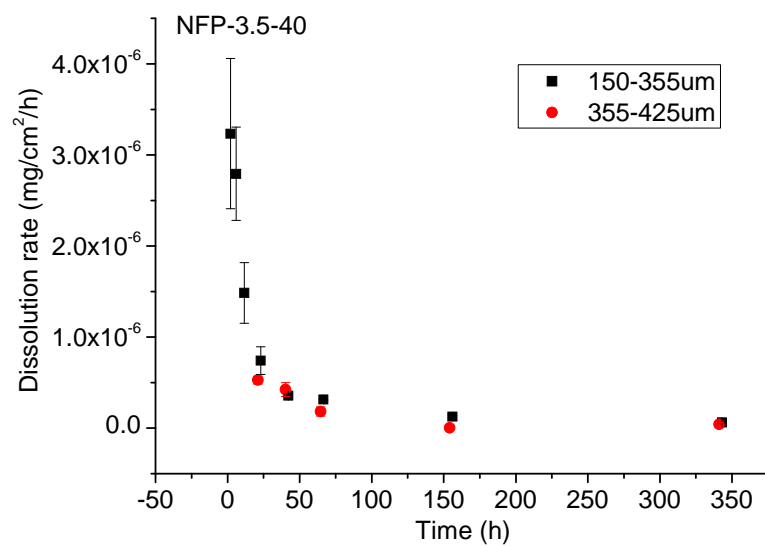
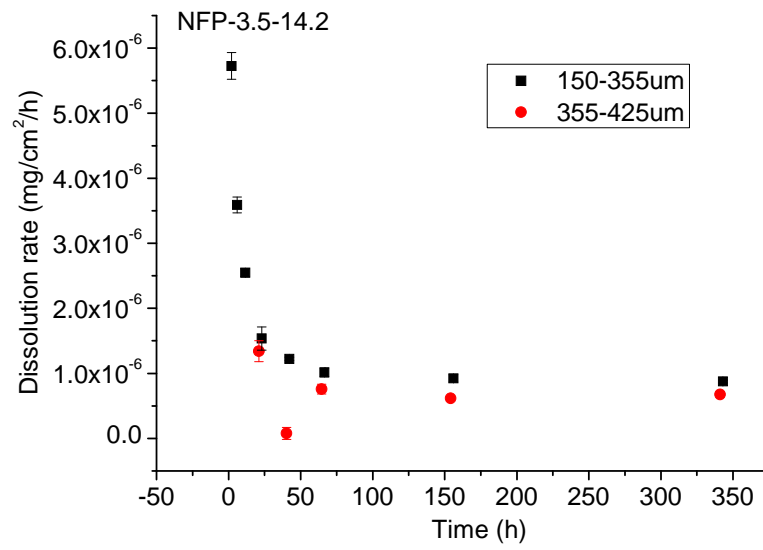


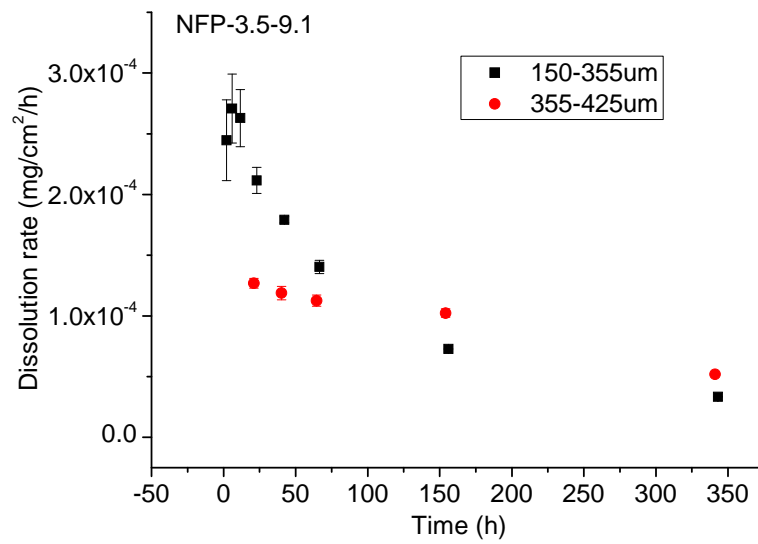
Fig. 32 (a)



(b)



(c)



(d)

Fig. 32(a-d) D_R of glass with O/P = 3.5 and varying particle size and time.

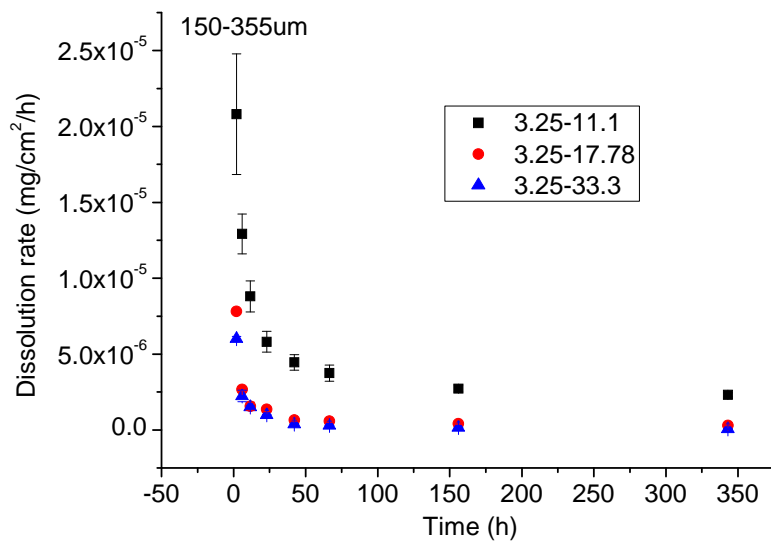
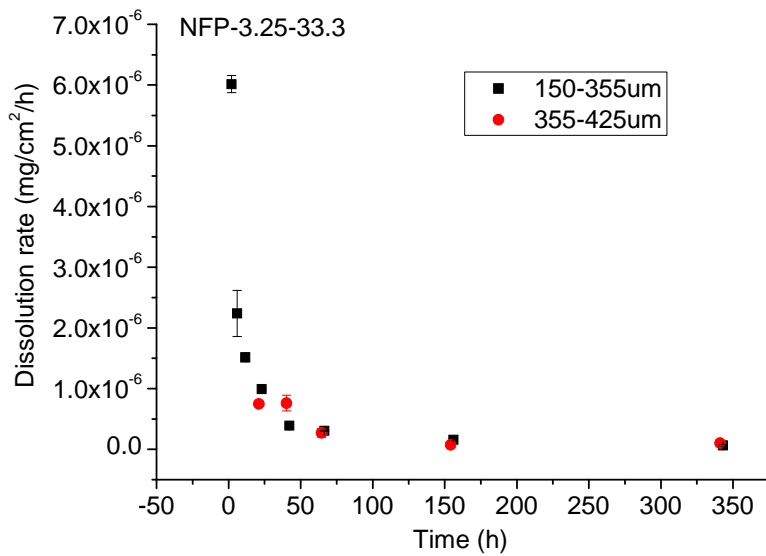
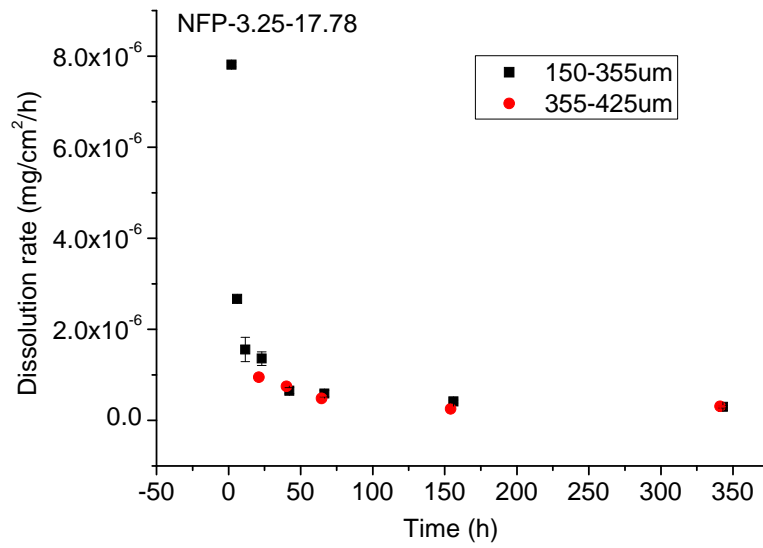


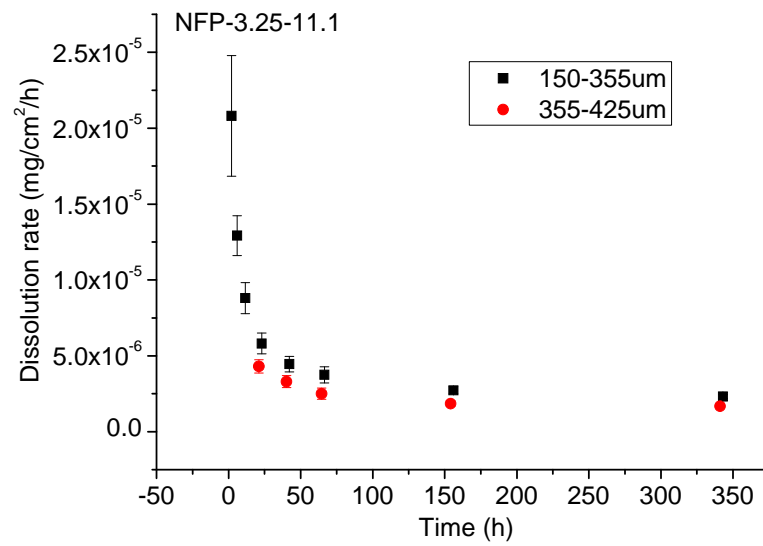
Fig. 33 (a)



(b)



(c)



(d)

Fig. 33(a-d) D_R of glass with O/P = 3.25 and varying particle size and time.

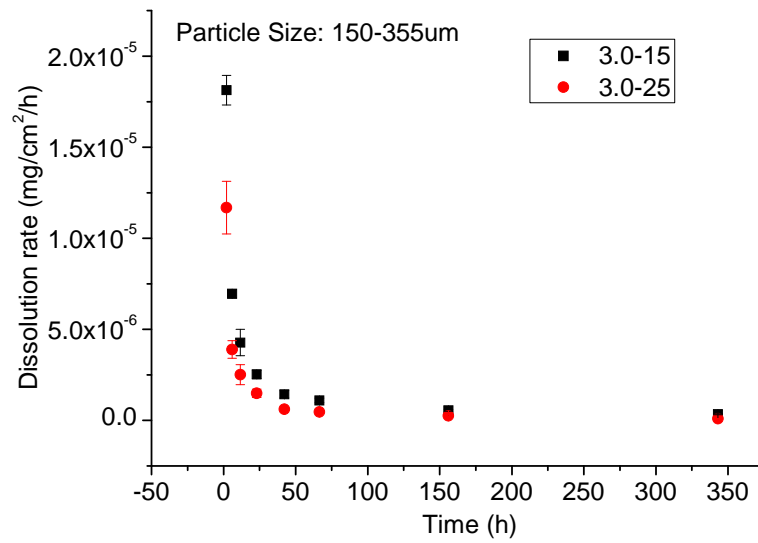
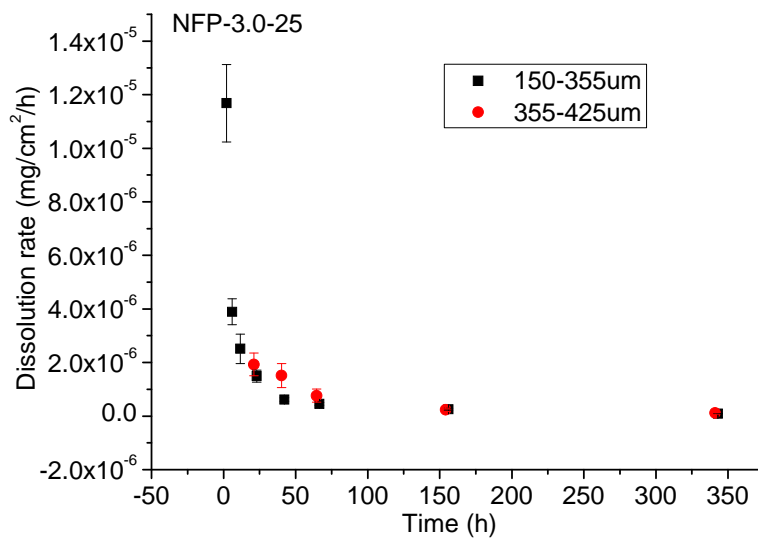
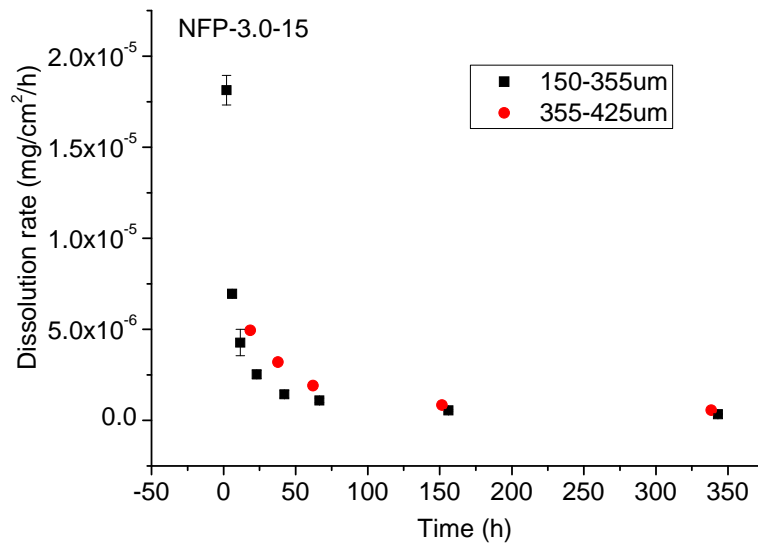


Fig. 34 (a)



(b)



(c)

Fig. 34(a-c) D_R of glass with O/P = 3.0 and varying particle size and time.

During dissolution of glasses NFP-3.25-11.1, NFP-3.0-15, NFP-3.5-14.2, and NFP-3.25-17.78, the ratio of Fe/P in the solution is similar to that of the original glass (Fig. 35). For all the other glasses (batched Na-free composition), dissolution of Fe is much less than that of Na-content glasses. Following are the dissolution amount (ppm) and pH value as function of time for each glass (Figs. 36–37).

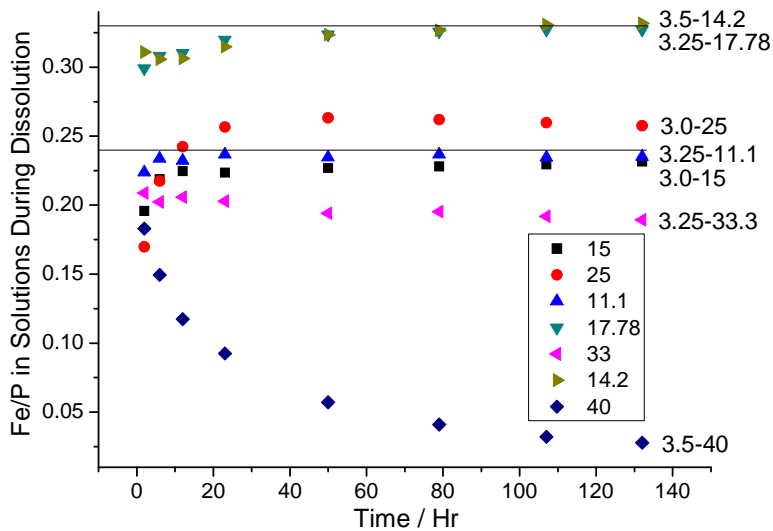


Fig. 35 Fe/P ratio change with time during dissolution process

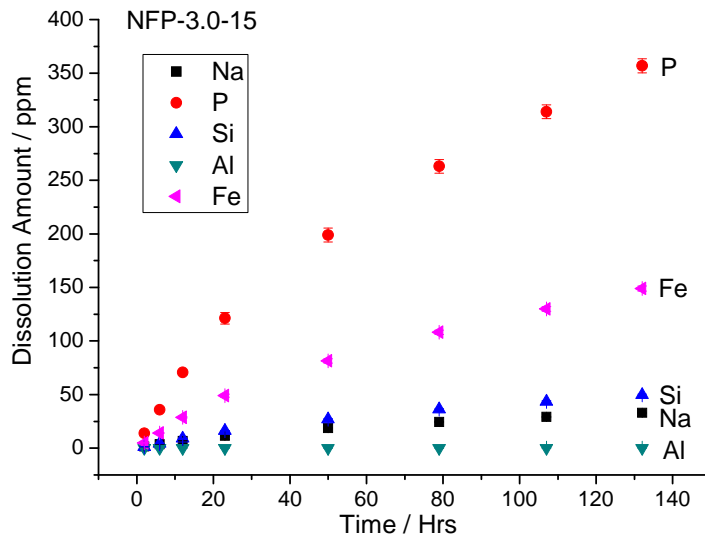
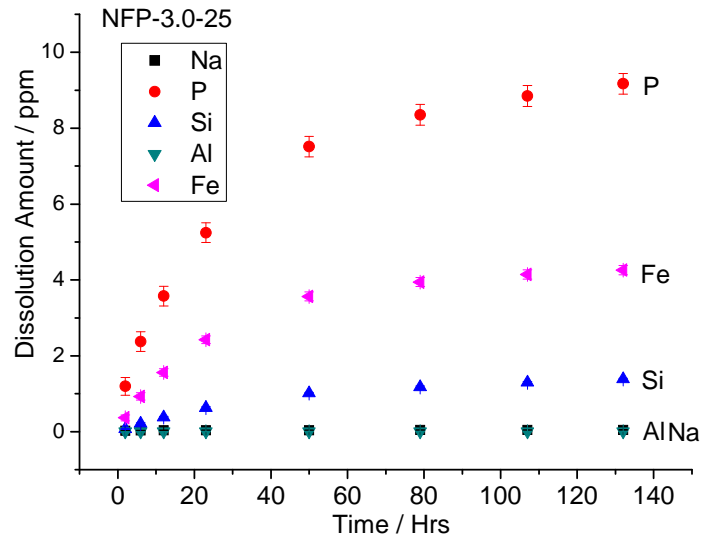


Fig. 36 (a)



(b)

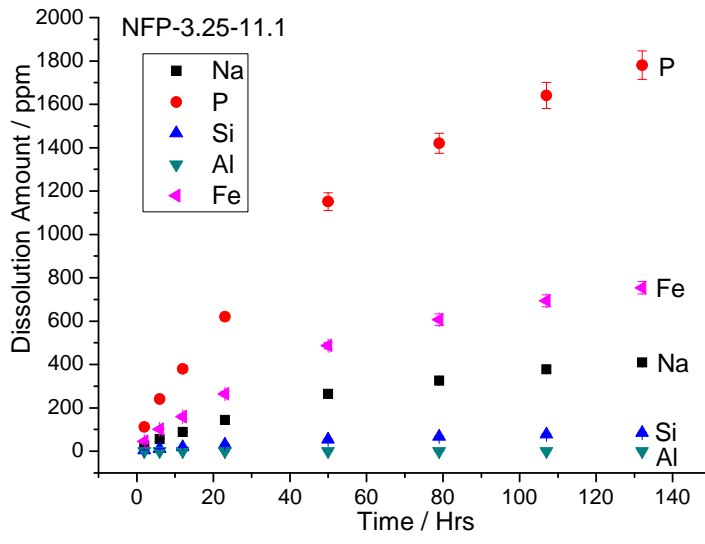
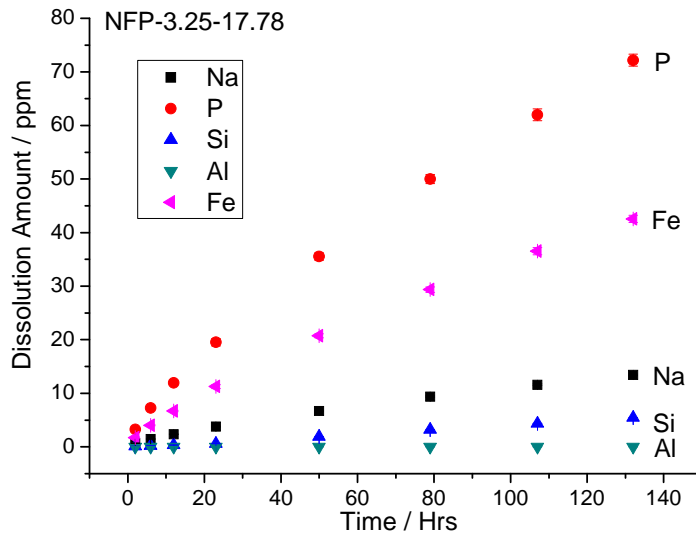


Fig. 36 (c)



(d)

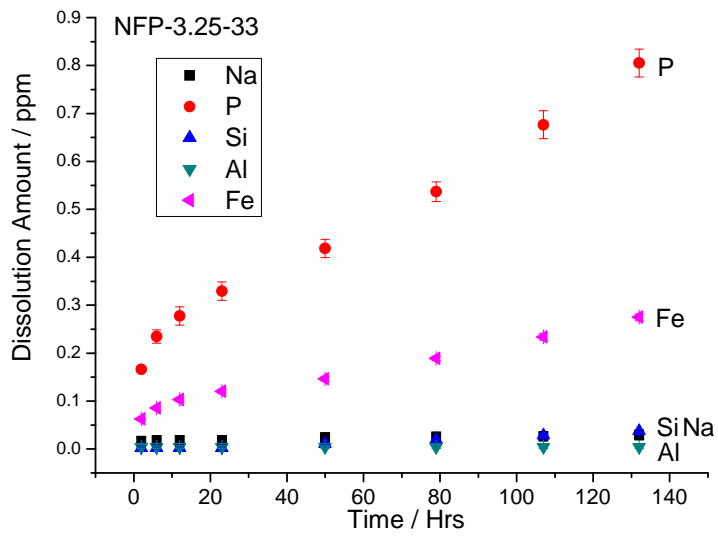
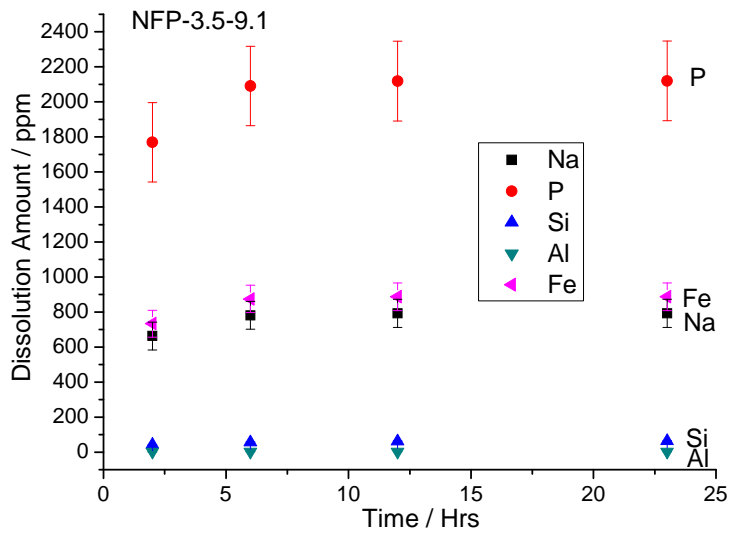
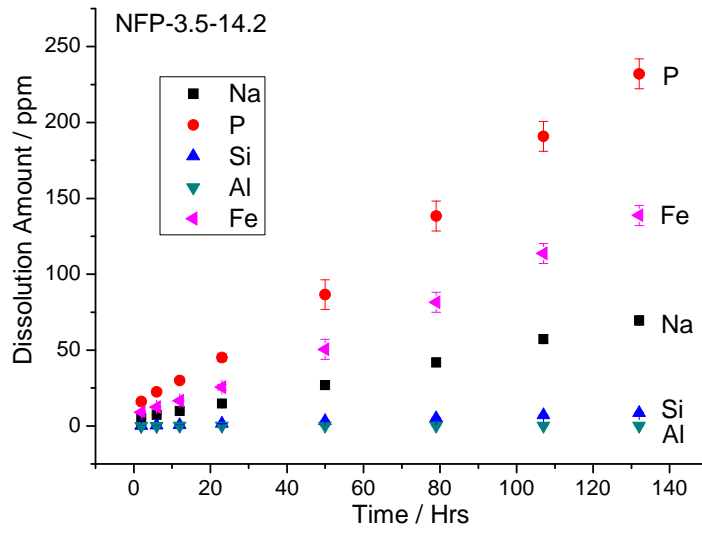


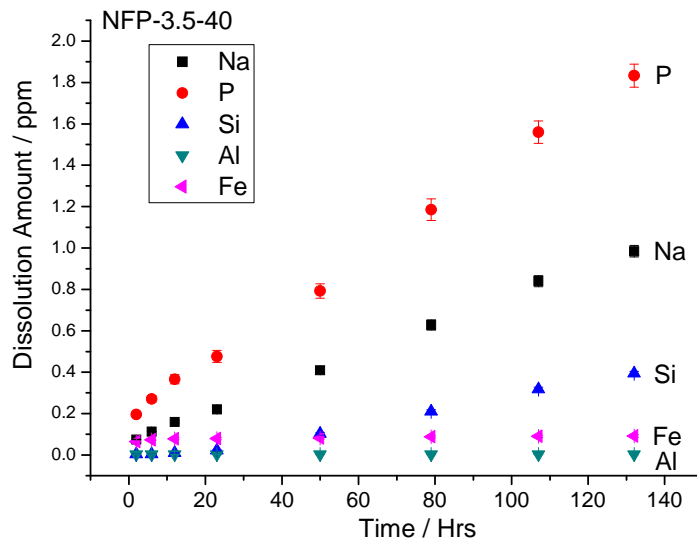
Fig. 36 (e)



(f)



(g)



(h)

Fig. 36(a-h) Dissolution amount (ppm) as function of time for each glass

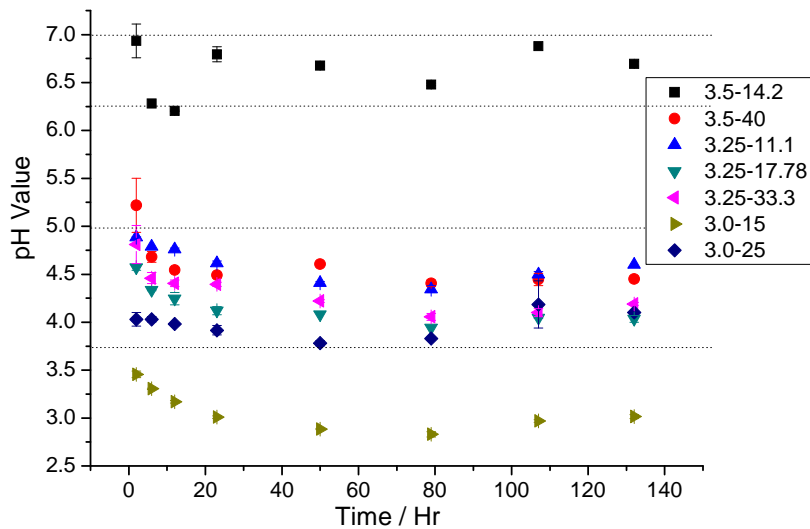


Fig. 37 pH value of dissolution solution after 140 hrs

Objective 2 – The Thermodynamic Properties of Iron Phosphate Compounds

I. Introduction

Modeling of corrosion rates in silicate glasses has suggested that these rates are a function of the Gibbs energy of dissolution of the glasses. This requires knowledge of the Gibbs energy of formation of the glass. Since this is difficult to determine experimentally, it is assumed that the Gibbs energy of formation of the glass equals the additive Gibbs energy of formation of the adjacent multiple oxide compounds, multiplied by their mole fraction in the glass. This relationship has only been proven in silicate glasses. Determining whether it is also the case in iron phosphate glasses requires knowing the Gibbs energy of formation of solid iron phosphate compounds, which have not been previously determined. To make this determination, a three-step experimental program was planned: (i) determination of the low-temperature (5–350 K) heat capacities of crystalline iron phosphate compounds, (ii) determination of the ambient-temperature enthalpies of formation of these compounds, and (iii) measurement of the high-temperature heat capacities of these compounds. The results of the three experimental programs are detailed below.

II. Low-Temperature Heat Capacity Measurement

(Q. Shi, B.F. Woodfield and J. Boerio-Goates, Department of Chemistry and Biochemistry, Brigham Young University)

1. Experimental Section

The heat capacity measurements were performed using a Quantum Design physical property measurement system (PPMS) in zero magnetic field over the temperature range from 1.9 K to 300 K. The PPMS measurement accuracy was determined by measuring a powdered copper and

benzoic acid to be $\pm 1\%$ from 22 K to 300 K and $\pm 2\%$ to $\pm 5\%$ below 22 K.¹ The procedure of powdered sample preparation for PPMS measurements and detailed experimental steps have already been reported previously.¹ In general, the powdered samples were prepared for the PPMS measurements by mixing them with Apiezon N grease in a copper cup which was then compressed into a pellet with a stainless steel die. The copper cup was formed from a foil of 0.025 mm thickness and 0.99999 mass fraction purity purchased from Alfa Aesar. The detailed measurement steps are: (1) Addenda measurement of the platform with Apiezon N grease. This grease will be used to thermally attach the copper cup to the platform. (2) Heat capacity measurement of a copper cup with Apiezon N grease inside the cup. This grease will be used to pot the sample inside the cup. (3) Combine the sample and Apiezon N grease in the copper cup, and then press them together into a pellet. (4) Another addenda measurement of the platform with Apiezon N grease. (5) Heat capacity measurement of the pellet. Steps (1) and (2) give the heat capacity of the copper cup and the grease, while steps (4) and (5) provide the heat capacity of the copper cup, the grease and the sample. The sample heat capacity can be calculated by subtracting the total heat capacities in step (2) from the total in step (5).¹

2. Results and C_p Data Fitting

The results of measured molar heat capacities of the iron phosphates are shown in Fig. 38. It can be seen from the heat capacity curves that each iron phosphate sample has a magnetic transition in the experimental temperature range from 1.9 K to 300 K.

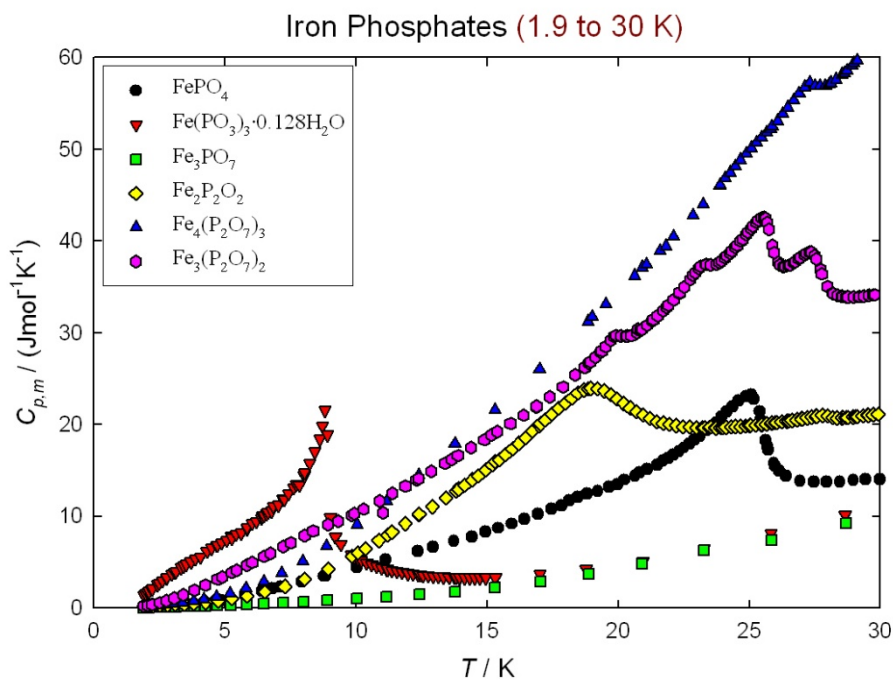
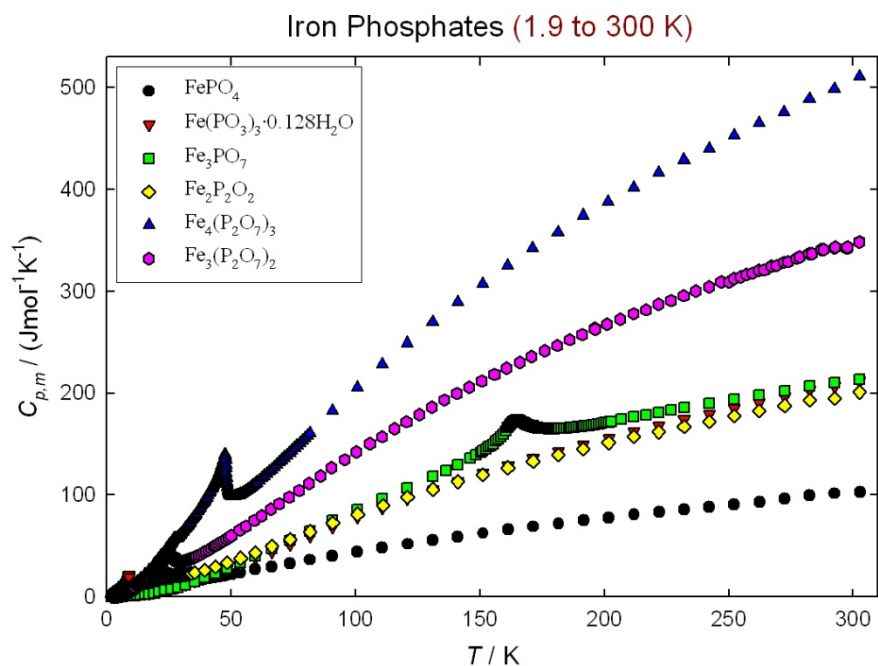


Fig. 38 (a)



(b)

Figure 38. Plot of experimental heat capacities against temperature for iron phosphates in the temperature range from $T = (1.9 \text{ to } 30) \text{ K}$ (a) and $T = (1.9 \text{ to } 300) \text{ K}$ (b).

To calculate the thermodynamic functions, we have performed curve fitting on the experimental data using different fitting methods in different temperature regions. In the low temperature region (below 10 K), the heat capacity data were fitted using a theoretical model of $C_{p,m} = \gamma * T + B_3 * T^3 + B_5 * T^5 + B_{asw} T^3 \exp(-\Delta/T) + B_{fasw} T^{3/2} \exp(-\Delta/T)$, where $\gamma * T$ is for electronic heat capacity, $B_3 * T^3 + B_5 * T^5$ for lattice contribution and $B_{asw} T^3 \exp(-\Delta/T) + B_{fasw} T^{3/2} \exp(-\Delta/T)$ for magnetic heat capacity contribution. The low temperature region fitting parameters are listed in Table IX. In the high temperature region (above 50 K), the heat capacity data were fitted by a combination of Debye and Einstein specific-heat functions: $C_{p,m} = n_D D(\theta_D) + n_E E(\theta_E)$, where $D(\theta_D)$ and $E(\theta_E)$ are Debye and Einstein functions, respectively. The high temperature region fitting parameters are given in Table X. In the middle temperature region (from 10 K to 50 K) and magnetic phase transition region, the heat capacity data were fitted using orthogonal polynomials and cubic spline polynomials, respectively. (Please see fitting reports for the details). Using these fitting parameters, we have calculated the standard molar thermodynamic functions for the iron phosphates at selected temperatures from $T \rightarrow 0 \text{ K}$ to $T = 300 \text{ K}$. The calculated results are given in attached excel files at the smoothed temperatures and at 298.15 K in Table XI.

Table IX. Parameters for fits below 10 K.

Parameters	Fe ₂ P ₂ O ₇	Fe ₃ (P ₂ O ₇) ₂	Fe ₃ PO ₇	Fe ₄ (P ₂ O ₇) ₃	Fe(PO ₃) ₃ · 0.128H ₂ O	FePO ₄
γ	8.40E-02		1.63E-02	7.37E-02	2.98E-01	
B_3	3.10E-03	3.76E-02	2.69E-03	7.42E-03	1.28E-01	3.77E-03
B_5	-1.50E-05	-3.89E-04	-4.05E-05	-5.83E-05		-3.95E-05
B_{asw}	1.10E-02		5.29E-02	1.88E-02		
B_{fsw}						2.92E-01
Δ	1.20E+01		3.19E+01	1.04E+01		8.54E+00
RMS%	0.69	6.61	1.65	1.14	0.017	6.88

Table X. Parameters for fits above 50 K

Parameters	Fe ₂ P ₂ O ₇	Fe ₃ (P ₂ O ₇) ₂	Fe ₃ PO ₇	Fe ₄ (P ₂ O ₇) ₃	Fe(PO ₃) ₃ · 0.128H ₂ O	FePO ₄
n_D	5.41	10.52	5.22	15.02	6.00	2.61
θ_D	344.6	380.4	334.7	374.7	390.6	301.3
n_E	5.56	9.00	5.62	13.6	6.09	2.81
θ_E	883.2	941.5	711.4	944.1	935.7	839.8
a						
b						
RMS%	0.57	0.34	1.19	0.46	0.43	0.29

Table XI. Standard Thermodynamic Functions at 298.15 K

Function	Fe ₂ P ₂ O ₇	Fe ₃ (P ₂ O ₇) ₂	Fe ₃ PO ₇	Fe ₄ (P ₂ O ₇) ₃	Fe(PO ₃) ₃ · 0.128H ₂ O	FePO ₄
$\frac{C_{p,m}^o}{J \cdot K^{-1} \cdot mol^{-1}}$	196.38	346.00	211.44	503.44	208.48	99.42
$\frac{S_m^o}{J \cdot K^{-1} \cdot mol^{-1}}$	220.50	384.12	219.73	561.03	215.69	119.20
$\frac{H(T)_m^o - H(0)_m^o}{kJ \cdot mol^{-1}}$	32.779	57.747	36.046	84.185	33.321	17.194

References

- (1) Shi, Q.; Snow, C. L.; Boerio-Goates, J.; Woodfield, B. F. *J. Chem. Thermodynamics* **2010**, *42*, 1107.

III. Enthalpy of Formation Determination

1. Parr Solution Calorimeter Measurements

Experiments were conducted on the use of a Parr solution calorimeter to determine the enthalpy of formation of iron phosphate compounds. Calibration of the instrument proceeded as desired; the instrument measures enthalpies of solution with about 3% uncertainty (Tables XII–XIV). However, measurements of the enthalpy of solution of sodium phosphate in HCl solutions did not yield results compatible to those achieved in previous acid–solution calorimetry experiments.

Table XII. Parr calorimeter dissolution of TRIS

Run	TRIS grams	6.0 N HCl grams	T _i °C	T _f °C	ΔT _c °C	.63R °C	T _{.63R} °C	QE Calories	e Cal/°C	e' Cal/°C
1	0.5024	100.0668	28.812	29.181	0.369	0.232	29.045	28.811	78.08	-21.88
2	0.5027	100.0653	28.3300	28.7030	0.3730	0.2350	28.565	28.911	77.51	-22.45
3	0.5072	100.0726	28.3120	28.7030	0.3910	0.2463	28.558	29.171	74.61	-25.36
4	0.5016	100.0932	28.8870	29.2650	0.3780	0.2381	29.125	28.753	76.07	-23.92
5	0.5072	100.0610	29.0800	29.4660	0.3860	0.2432	29.323	29.037	75.23	-24.73
6	0.5087	100.0571	28.9090	29.2910	0.3820	0.2407	29.15	29.157	76.33	-23.62
Avg.							28.961		76.30	-23.67
									SD: 1.20	

The initial quality assurance test of the calorimeter was to reproduce the experimentally measured enthalpies of other phosphate compounds. This would be done by measuring the enthalpy of dissolution of a basic oxide and P₂O₅, mixed in the stoichiometrically appropriate ratio, and then measure the enthalpy of dissolution of the phosphate compound. The difference is the enthalpy of formation of the compound from the oxides.

Table XIII. Parr calorimeter dissolution of CaO

	CaO grams	6N HCl grams	T _i °C	T _f °C	ΔT _c °C	.63R °C	T _{0.63R} °C	Q Calories	e Cal/°C	Enthalpy Change kJ/mole
run #1	0.301	100.055	27.429	28.971	1.5420	0.9715	28.4005	117.655	76.30	-91.61
run #2	0.301	100.044	27.189	28.721	1.5320	0.9652	28.1542	116.892	76.30	-91.16
run #3	0.303	100.033	27.284	28.840	1.5560	0.9803	28.2643	118.723	76.30	-91.97
Average							28.2730			-91.58

Table XIV. Parr calorimeter dissolution of P₂O₅

Run	P ₂ O ₅ grams	6N HCl grams	T _i °C	T _f °C	ΔT _c °C	.63R °C	T _{.63R} °C	Q Calories	e Cal/°C	Enthalpy Change kJ/mole
1	0.3000	100.0521	26.969	27.736	0.767	0.4832	27.4522	58.522	76.30	-115.85
2	0.3000	100.0432	26.767	27.532	0.765	0.4820	27.2490	58.370	76.30	-115.55
3	0.3200	100.0327	26.812	27.652	0.840	0.5292	27.3412	64.092	76.30	-118.95
4	0.3200	100.0527	26.862	27.599	0.737	0.4643	27.3263	56.233	76.30	-104.36
Avg							27.3422			-115.70

Within its limitations (discussed later), the calorimeter performed well. Experiments dissolving a mixture of CaO and P₂O₅ in 6N HCl yielded reproducible enthalpies of solution, with an uncertainty of about 3%. However, the calcium phosphate compound used as a reference (Ca₂P₂O₇) failed to dissolve in appreciable quantities at room temperature.

Table XV. Parr calorimeter dissolution of γ-CaP₂O₇

Run	Ca ₂ P ₂ O ₇ Grams	6N HCl Grams	T _i °C	T _f °C	ΔT _c °C	.63R °C	T _{.63R} °C	Q Calo- ries	e Calories/ °C	Enthalpy Change kJ/mole
1	0.5045	100.057	26.941	27.039	0.098	0.062	27.0027	7.477	76.30	-15.76
2	0.5074	100.039	27.115	27.203	0.088	0.055	27.1704	6.714	76.30	-14.07
3	0.5081	100.026	27.714	27.816	0.102	0.064	27.7783	7.783	76.30	-16.28
Avg.							27.3171			-15.37

The difficulty lies in proving that the instrument can be used to reproduce existing enthalpies of formation for phosphate compounds. The calorimeter operates only at ambient temperature, and the solubility of many phosphates appears to be strongly temperature-dependent, even in 6N HCl. Between this and the limited number of phosphate compounds for which reliable enthalpies of formation have been determined, it was difficult to find a 'test' reaction which worked in the calorimeter.

Another problem that became apparent was with hydration of samples during transfer have made it apparent that direct measurement of the enthalpy of formation of iron phosphate compounds from the constituent oxides could not be achieved. Instead it would be necessary to use an indirect reaction such as Na₃PO₄ + FeCl₃ = FePO₄ + 3 NaCl to obtain enthalpies of formation instead.

Attempts to dissolve the phosphate in acid at 35 °C proved more successful. However, the Parr calorimeter is not designed to operate at temperatures other than ambient, and there is no way of maintaining other temperatures in the system. As a result, the thermal effect resulting from cooling of the solution during experiments ruined the reproducibility of the results. Attempts were made to dissolve other calcium phosphates in the room--temperature acid, without success; and

attempts were made to determine the enthalpy of formation of lithium phosphates using a similar approach. None of these were successful. The use of lithium and other phosphates introduces an additional potential source of error, since many of these compounds are hygroscopic. To account for this, the calorimeter was kept in a glove box, and students became adept at quick transfer of contents from the weighing dish to the calorimeter. However, none of this seemed to work well, and the conclusion was reached that accurate measurement of enthalpies of formation of iron phosphates in this calorimeter is not feasible.

As a result of these failures, an alternate method was sought to obtain the enthalpies of formation of iron phosphate compounds. Work has also begun on calculating iron phosphate enthalpies of formation, using first-principles methods. Prof. Julia Medvedeva in the Department of Physics at Missouri S&T began making such calculations, based on measured crystal structures for the different compounds.

2. Formation energy of Fe-P-O compounds

We employed first-principles density functional approach within all-electron full-potential linearized augmented plane wave (FLAPW) method [1,2] with the generalized gradient density approximation (GGA) for accurate total energy calculations of the Fe-P-O compounds. We note that GGA is known to give improved results for transition-metal-containing compounds compared to the standard local density approximation (LDA) which assumes a uniform electron density distribution. Cutoffs for the plane wave basis functions, 16.0 Ry, and potential representation, 81.0 Ry, and expansion in terms of spherical harmonics with $l \leq 8$ inside the muffin-tin spheres were used. The muffin-tin radii are 2.20 a.u. for Fe; 1.40 a.u. for P; and 1.25-1.40 a.u. for O atoms. Summations over the Brillouin zone were carried out using at least 23 special \mathbf{k} points in the irreducible wedge.

The crystal structure data for the five Fe-P-O compounds were taken from the Inorganic Crystal Structure Database (ICSD). Because the atomic forces were large for every structure, the internal positions of all atoms in the unit cells were optimized via the total energy and atomic forces minimization. During the optimization, the lattice parameters were fixed at the experimental values.

To calculate the formation energy of the iron phosphates, we have calculated the total energy of bulk bcc Fe and triclinic P (space group P_1 , with 24 atoms per unit cell) as well as the total energy of the O_2 molecule. The formation energies were calculated according to the following equation:

$$E_{\text{form}}(\text{Fe}_x\text{P}_y\text{O}_z) = E_{\text{tot}}(\text{Fe}_x\text{P}_y\text{O}_z) - x E_{\text{tot}}(\text{Fe}) - y E_{\text{tot}}(\text{P})/24 - z E_{\text{tot}}(\text{O}_2)/2 \quad (2)$$

The results, listed in Table XVI, are given per formula unit. It is seen, that the results are in reasonable agreement with the formation energies found in literature with exception for $\text{Fe}_2\text{P}_2\text{O}_7$ and $\text{Fe}_4(\text{P}_2\text{O}_7)_3$. We believe that the formation energy underestimation for the latter two compounds is due to the non-magnetic solutions obtained in our calculations. These low-symmetry structures possess a complex magnetic ordering which require supercell calculations to take into account the correct magnetic interactions. Therefore, magnetism plays an important role in the

formation of the Fe-P-O compounds and their polymorphs, and should be taken into account for accurate energy calculations.

Table XVI. Calculated formation energies (in eV) and Fe magnetic moments (in μ_B) of five Fe-P-O compounds.					
Compound	Space group	Z	E_{FORM} (this work)	E_{FORM} (earlier works)	Mag. moment
FePO₄	Orthorhombic, Pnma	4	-18.02	-15.31	4.08
Fe(PO₃)₃	Monoclinic, C ₁ C ₁	6	-41.38	-33.95	4.14
Fe₃PO₇	Rhombohedral, R3m	1	-29.08	-26.08	4.07
Fe₂P₂O₇	Triclinic, P ₁	1	-28.49	-29.10	0
Fe₄(P₂O₇)₃	Monoclinic, P ₁ 2 ₁ /n1	4	-61.10	-80.17	0

[1] E. Wimmer, H. Krakauer, M. Weinert, and A.J. Freeman, Full-potential self-consistent linearized-augmented-plane-wave method for calculating the electronic structure of molecules and surfaces - O₂ molecule. Phys. Rev. B **24**, 864-875 (1981).

[2] M. Weinert, E. Wimmer, and A.J. Freeman, Total-energy all-electron density functional method for bulk solids and surfaces. Phys. Rev. B **26**, 4571-4578 (1982).

3. High-Temperature Heat Capacity Measurements

A third element of the experimental determination of iron phosphate thermodynamic properties was measurement of high-temperature heat capacities, using the Netzsch STA 409 instrument at Missouri S&T. This instrument is theoretically capable of accurate and reproducible measurement up to 1400 °C. However, early in the experimental program the closure of the Graduate Center for Materials Research at Missouri S&T for renovation required relocation of the instrument to another building. When repeated attempts were made to use the relocated instrument for heat capacity measurement, it proved impossible to generate a reproducible baseline, much less reproducible measurement of heat capacity for an unknown compound. It is suspected that building noise is to blame, and that the instrument will not be usable for this task until it is relocated to its original home in the renovated MRC. In the meantime, iron phosphate samples have been sent to Netzsch for testing on a new high-temperature instrument; it is hoped to use the results from these experiments for calculation of above-ambient iron phosphate thermodynamic properties

Future Work

Objective 1.

Corrosion studies remain to be conducted on the 25-25-50 Na₂O-CaO-P₂O₅ glass in powder form (150–300 μ m) at 25, 50, and 100 °C. Iron phosphate glass 31-17 will be tested in bulk with 0.1M HCl, 0.1M KOH, and DI H₂O, and in powder form in 0.1M KOH and DI H₂O. Articles for publication are currently in preparation.

Objective 2.

The results of the low-temperature heat-capacity measurements and the first-principles measurement of enthalpies of formation for iron phosphate compounds will be combined to generate estimated Gibbs energies of formation of these compounds. These in turn will be used to estimate the Gibbs energies of formation of the iron phosphate glasses produced for this study. The known thermodynamic properties of calcium and sodium phosphate compounds will similarly be used to calculate Gibbs energies of formation for the $\text{Na}_2\text{O-CaO-P}_2\text{O}_5$ glasses studied under Objective 1. High-temperature heat capacity measurements for iron phosphate compounds are currently being performed by the equipment manufacturer, and we hope to see these results in the near future as well.

The ultimate goal will be to determine if the corrosion rates of phosphate glasses can be predicted as a function of the Gibbs energy of dissolution of the glasses.